

Temperature-dependent cross sections for charmonium dissociation in collisions with pions and rhos in hadronic matter

Jie Zhou Xiao-Ming Xu

Department of Physics, Shanghai University, Baoshan, Shanghai 200444, China

Abstract

Meson-charmonium dissociation reactions governed by the quark interchange are studied with temperature-dependent quark potentials. Quark-antiquark relative-motion wave functions and masses of charmonia and charmed mesons are determined by the central spin-independent part of the potentials or by the central spin-independent part and a smeared spin-spin interaction. The prominent temperature dependence of the masses is found. Based on the potentials, the wave functions, and the meson masses, we obtain temperature-dependent cross sections for the fifteen dissociation reactions: $\pi J/\psi \rightarrow \bar{D}^* D$ or $\bar{D} D^*$, $\pi J/\psi \rightarrow \bar{D}^* D^*$, $\pi \psi' \rightarrow \bar{D}^* D$ or $\bar{D} D^*$, $\pi \psi' \rightarrow \bar{D}^* D^*$, $\pi \chi_c \rightarrow \bar{D}^* D$ or $\bar{D} D^*$, $\pi \chi_c \rightarrow \bar{D}^* D^*$, $\rho J/\psi \rightarrow \bar{D} D$, $\rho J/\psi \rightarrow \bar{D}^* D$ or $\bar{D} D^*$, $\rho J/\psi \rightarrow \bar{D}^* D^*$, $\rho \psi' \rightarrow \bar{D} D$, $\rho \psi' \rightarrow \bar{D}^* D$ or $\bar{D} D^*$, $\rho \psi' \rightarrow \bar{D}^* D^*$, $\rho \chi_c \rightarrow \bar{D} D$, $\rho \chi_c \rightarrow \bar{D}^* D$ or $\bar{D} D^*$, and $\rho \chi_c \rightarrow \bar{D}^* D^*$. The numerical cross sections are parametrized for future applications in hadronic matter. The particular temperature dependence of the J/ψ bound state leads to unusual behavior of the cross sections for endothermic J/ψ dissociation reactions. The quantum numbers of ψ' and χ_c can not make their difference in mass in the temperature region $0.6T_c \leq T < T_c$, but can make the ψ' dissociation different from the χ_c dissociation.

PACS: 25.75.Nq, 12.39.Jh, 13.75.Lb

Keywords: Dissociation cross section; Quark-interchange mechanism; Quark potential model.

1. Introduction

From the year when Matsui and Satz [1] originally suggested the suppressed J/ψ production as a signature for the formation of a quark-gluon plasma in high-energy heavy-ion collisions to the last year's quark matter conference where preliminary J/ψ data in Pb-Pb collisions at the Large Hadron Collider were reported by the ALICE Collaboration [2] and the CMS Collaboration [3], important measurements have been done. Essential theoretical progress on J/ψ has also been made. One of the fundamental issues is the dissociation of charmonia in hadronic matter [4]. To identify J/ψ as a probe of the quark-gluon plasma in a definite way, hadron-charmonium dissociation processes must be well understood. Calculations of dissociation cross sections are thus an important aspect in studying J/ψ physics. The dissociation is described by the meson or quark degree of freedom. Corresponding to the two degrees of freedom, different scattering mechanisms can be assumed, and different results on the dissociation cross sections have been reported in the literature.

There are mainly three approaches to the meson- J/ψ dissociation problem. In the short-distance approach the parton model of light hadrons, the constituent quark model of J/ψ , and the gluon- J/ψ dissociation cross section of Peskin and Bhanot [5] are employed in Refs. [6, 7] to investigate $\pi J/\psi$ and $N J/\psi$ dissociation. The portion of hard gluons inside the nucleon or pion at low energies is not large enough to induce mb-scale cross sections. In the meson-exchange approach J/ψ dissociation has been studied with effective meson Lagrangians. Since the discovery of J/ψ reveals the charm quark, J/ψ is first described by QCD. The meson field description of J/ψ and charmed mesons began to appear from the work of Matinyan and Müller [8] who first discussed the t-channel exchange of D meson in inelastic $\pi J/\psi$ and $\rho J/\psi$ scattering. They got mb-scale cross sections for $\pi J/\psi \rightarrow D^* \bar{D} + D \bar{D}^*$ and $\rho J/\psi \rightarrow D \bar{D}$ at low energies. A similar scale of cross sections has been obtained in other meson Lagrangians with different symmetries and modified vertex functions in Feynman diagrams to include the effect of finite meson form factors [9–14]. In the quark-interchange approach J/ψ dissociation has been studied in nonrelativistic quark

potential models [15–18]. The assumption that color-independent confining interaction acts only between a quark and an antiquark in Ref. [15] yields that the J/ψ absorption cross section corresponding to $\pi J/\psi \rightarrow D^* \bar{D} + D \bar{D}^* + D^* \bar{D}^*$ has a peak value of about 7 mb at the kinetic energy $E_{\text{kin}} \equiv \sqrt{s} - (m_\pi + m_{J/\psi}) \simeq 0.8$ GeV. However, by including color generators in the linear confining potential and allowing the interaction to connect any two constituents (quarks and antiquarks), Wong, Swanson, and Barnes [16] gave a peak value of only ~ 1 mb at the same kinetic energy. Usefully, the dissociation cross sections of ground state, orbitally and radially excited charmonia in collisions with π and ρ mesons have been presented in Ref. [18] where all parameters in the color Coulomb, spin-spin hyperfine and linear confining interactions are determined by fits to the experimental meson spectrum.

All the above works only involve charmonium dissociation reactions in vacuum, and have been used to evaluate J/ψ suppression in nucleus-nucleus collisions, but we know that hadron masses, the quark potential and so on are affected by medium and the QCD phase transition is the most striking medium effect, so we must study medium effects on the charmonium dissociation. In this work we calculate dissociation cross sections of J/ψ , ψ' , and χ_c in collisions with π and ρ at various temperatures. The quark-interchange mechanism [19], the Born approximation, and a temperature-dependent quark potential [20] are ingredients in establishing cross section formulas.

This paper is organized as follows. In the next section we use the temperature-dependent potential [20] in the Schrödinger equation to obtain temperature-dependent masses of charmonia and charmed mesons. In Section 3 we give formulas for charmonium dissociation cross sections. Numerical results for unpolarized cross sections of J/ψ , ψ' , and χ_c in collisions with π and ρ at six temperatures are shown in Section 4 and relevant discussions are given. In Section 5 the spin-spin interaction arising from one-gluon exchange is smeared. Subsequent results are shown and numerical cross sections are parametrized. In Section 6 we present a procedure on how to obtain unpolarized cross sections at any temperature in the region $0.65 \leq T/T_c < 1$ where T_c is the critical temperature. Finally, we summarize the present work in Section 7.

2. Masses of charmonia and charmed mesons

As shown in Refs. [21–24], the quark potential containing flavor-independent confinement, a Coulomb term and hyperfine interactions can consistently reproduce masses from light to heavy hadrons, and the flavor-independent assumption of confinement is thus reasonable. Such confinement in hadronic matter can be estimated by the lattice calculations [25] and depends on temperature. At large distances the confinement manifests itself by a plateau that lowers with increasing temperature. In Ref. [20] we used the confinement at large distances and the short-distance potential originating from one-gluon exchange and loop corrections in perturbative QCD [26] to construct a central spin-independent, flavor-independent but temperature-dependent potential

$$V_{\text{si}}(\vec{r}) = -\frac{\vec{\lambda}_a}{2} \cdot \frac{\vec{\lambda}_b}{2} \frac{3}{4} D \left[1.3 - \left(\frac{T}{T_c} \right)^4 \right] \tanh(Ar) + \frac{\vec{\lambda}_a}{2} \cdot \frac{\vec{\lambda}_b}{2} \frac{6\pi}{25} \frac{v(\lambda r)}{r} \exp(-Er). \quad (1)$$

Only here $D = 0.7$ GeV, $T_c = 0.175$ GeV, $A = 1.5[0.75 + 0.25(\frac{T}{T_c})^{10}]^6$ GeV, $E = 0.6$ GeV, and $\lambda = \sqrt{3b_0/16\pi^2\alpha'}$ in which $\alpha' = 1.04$ GeV⁻² is the Regge slope and $b_0 = 11 - \frac{2}{3}N_f$ with the quark flavor number $N_f = 4$. $\vec{\lambda}_a$ are the Gell-Mann matrices for the color generators of constituent a . The dimensionless function $v(x)$ is an integration over the absolute value of gluon momentum \vec{Q}

$$v(x) = \frac{4b_0}{\pi} \int_0^\infty \frac{dQ}{Q} (\rho(\vec{Q}^2) - \frac{K}{\vec{Q}^2}) \sin(\frac{Q}{\lambda}x), \quad (2)$$

where $K = 3/16\pi^2\alpha'$. The subtraction of K/\vec{Q}^2 from the physical running coupling constant $\rho(\vec{Q}^2)$ leaves only the contribution of one-gluon exchange plus perturbative one- and two-loop corrections. The factor $\exp(-Er)$ is a medium modification factor to the potential of one-gluon exchange plus perturbative one- and two-loop corrections. The temperature dependence is completely negligible at very short distances and obvious at intermediate and large distances. The potential well fits the lattice gauge results at $T/T_c > 0.55$ [25], but fails to give a long-ranged linear confining potential at $T = 0$.

Given the charm quark mass $m_c = 1.51$ GeV, the Schrödinger equation with the potential given in Eq. (1) is solved to obtain masses and wave functions of J/ψ , ψ' , and χ_c . Here the χ_c mass corresponds to the center of gravity of χ_{c0} , χ_{c1} , and χ_{c2} [27]. At

$T = 0$ the masses of J/ψ , ψ' , and χ_c are 3.10505 GeV, 3.67679 GeV, and 3.51138 GeV, compared to the experimental values 3.096916 GeV, 3.68609 GeV, and 3.5253 GeV [28], respectively. The temperature dependence of the charmonium masses is shown by the solid, dashed and dotted curves in Fig. 1. Because J/ψ has a small radius, the J/ψ mass changes more slowly than the ψ' and χ_c masses. Even though ψ' and χ_c have different quantum numbers, both become degenerate in mass in the temperature region in Fig. 1. Furthermore, at temperatures very close to the critical temperature J/ψ joins ψ' and χ_c to form a triplet in mass. This is a medium effect on charmonia!

Given $m_c = 1.51$ GeV, the up and down quark masses $m_u = m_d = 0.32$ GeV, and the strange quark mass $m_s = 0.5$ GeV, the Schrödinger equation with the central spin-independent potential offers the same quark-antiquark relative-motion wave functions of π and ρ (D and D^* , D_s and D_s^*) and the spin-averaged mass of π and ρ (D and D^* , D_s and D_s^*). The spin-averaged mass of a spin-0 meson and a spin-1 meson with the same isospin is one-fourth of the spin-0 meson mass plus three-fourths of the spin-1 meson mass. The quark-antiquark relative-motion wave functions of π and ρ (D and D^* , D_s and D_s^*) are used to calculate the mass splitting of π and ρ (D and D^* , D_s and D_s^*) with the spin-spin interaction that arises from one-gluon exchange plus one- and two-loop corrections [29]

$$V_{ss} = -\frac{\vec{\lambda}_a}{2} \cdot \frac{\vec{\lambda}_b}{2} \frac{16\pi^2}{25} \delta^3(\vec{r}) \frac{\vec{s}_a \cdot \vec{s}_b}{m_a m_b} + \frac{\vec{\lambda}_a}{2} \cdot \frac{\vec{\lambda}_b}{2} \frac{4\pi}{25} \frac{1}{r} \frac{d^2 v(\lambda r)}{dr^2} \frac{\vec{s}_a \cdot \vec{s}_b}{m_a m_b}, \quad (3)$$

where \vec{s}_a (\vec{s}_b) and m_a (m_b) are the spin and mass of the constituent a (b), respectively. From the mass splitting and the spin-averaged mass we get the spin-0 meson mass and the spin-1 meson mass: the former is the spin-averaged mass minus three-fourths of the mass splitting; the latter is the spin-averaged mass plus one-fourth of the mass splitting. At $T = 0$ the masses of D , D^* , D_s , and D_s^* are 1.80666 GeV, 2.09552 GeV, 1.85228 GeV, and 2.18695 GeV, compared to the measured values 1.86722 GeV, 2.00861 GeV, 1.96847 GeV, and 2.1123 GeV, respectively. The temperature dependence of the D , D^* , D_s and D_s^* masses is plotted in Fig. 1 as two long dashed curves and two dot-dashed curves. The D and D_s masses keep almost unchanged from $T = 0.6T_c$ to $0.85T_c$ and $0.9T_c$, respectively, and apparently fall off in the other temperature regions. The D^* and D_s^*

masses decrease slowly from $T = 0.6T_c$, and become apparently falling off from $T = 0.8T_c$ and $T = 0.85T_c$, respectively. The medium effect on charmed mesons is obvious only in the region where the masses apparently fall off. The temperature dependence of π and ρ masses was shown in Fig. 2 of Ref. [20]. With increasing temperature the π mass decreases slowly for $0.6T_c \leq T < 0.78T_c$ and rapidly for $T \geq 0.78T_c$ while the ρ mass decreases rapidly for $0.6T_c \leq T < T_c$. From $T = 0.6T_c$ to $0.99T_c$ the masses of π , ρ , J/ψ , ψ' , χ_c , D , D^* , D_s , and D_s^* are reduced by 100%, 99%, 7%, 16%, 16%, 20%, 27%, 12%, and 23%, respectively. Therefore, the medium effect on the two light mesons is more obvious. Either D and D^* or D_s and D_s^* become a doublet in mass at $T \rightarrow T_c$, but the four mesons do not become degenerate unlike J/ψ , ψ' and χ_c .

The meson masses in units of GeV in the region $0.6 \leq T/T_c < 1$ are parametrized as

$$m_{J/\psi} = 3.07 \left[1 - \left(\frac{T}{1.01T_c} \right)^{3.76} \right]^{0.03}, \quad (4)$$

$$m_{\psi'} = 3.48 \left[1 - \left(\frac{T}{2.19T_c} \right)^{4.63} \right]^{7.74}, \quad (5)$$

$$m_{\chi_c} = 3.42 \left[1 - \left(\frac{T}{1.89T_c} \right)^{5.65} \right]^{6.96}, \quad (6)$$

$$m_D = 1.795 \left[1 - \left(\frac{T}{1.16T_c} \right)^{9.67} \right]^{0.92}, \quad (7)$$

$$m_{D^*} = 2.02 \left[1 - \left(\frac{T}{1.42T_c} \right)^{5.38} \right]^{2.18}, \quad (8)$$

$$m_{D_s} = 1.94 \left[1 - \left(\frac{T}{1.02T_c} \right)^{3.3} \right]^{0.08}, \quad (9)$$

$$m_{D_s^*} = 2.133 \left[1 - \left(\frac{T}{1.29T_c} \right)^{6.28} \right]^{1.29}. \quad (10)$$

3. Cross section formulas

In nonrelativistic dynamics for the quark-interchange process $q\bar{q} + c\bar{c} \rightarrow q\bar{c} + c\bar{q}$, the center-of-mass motion of $q\bar{q}$ and $c\bar{c}$ (i.e. $q\bar{c}$ and $c\bar{q}$) is separated off. This guarantees

that cross sections are calculated in a way independent of the center of mass. We then choose the center-of-mass frame where the cross section can be easily formulated [30]. We denote the mass and the four-momentum of meson i ($i = q\bar{q}, c\bar{c}, q\bar{c}, c\bar{q}$) by m_i and $P_i = (E_i, \vec{P}_i)$, respectively. The Mandelstam variables are $s = (E_{q\bar{q}} + E_{c\bar{c}})^2 - (\vec{P}_{q\bar{q}} + \vec{P}_{c\bar{c}})^2$ and $t = (E_{q\bar{q}} - E_{q\bar{c}})^2 - (\vec{P}_{q\bar{q}} - \vec{P}_{q\bar{c}})^2$. The cross section for the meson-charmonium scattering $q\bar{q} + c\bar{c} \rightarrow q\bar{c} + c\bar{q}$ in the center-of-mass frame is

$$\sigma(S, m_S, \sqrt{s}, T) = \frac{1}{32\pi s} \frac{|\vec{P}'(\sqrt{s})|}{|\vec{P}(\sqrt{s})|} \int_0^\pi d\theta |\mathcal{M}_{\text{fi}}(s, t)|^2 \sin \theta, \quad (11)$$

where S is the total spin of either the two incoming mesons or the two outgoing mesons, m_S is the magnetic projection quantum number of S , \mathcal{M}_{fi} is the transition amplitude, and θ is the angle between $q\bar{q}$ momentum \vec{P} and $q\bar{c}$ momentum \vec{P}' . \vec{P} and \vec{P}' are related to the Mandelstam variable s by

$$\vec{P}^2(\sqrt{s}) = \frac{1}{4s} \left\{ [s - (m_{q\bar{q}}^2 + m_{c\bar{c}}^2)]^2 - 4m_{q\bar{q}}^2 m_{c\bar{c}}^2 \right\}, \quad (12)$$

$$\vec{P}'^2(\sqrt{s}) = \frac{1}{4s} \left\{ [s - (m_{q\bar{c}}^2 + m_{c\bar{q}}^2)]^2 - 4m_{q\bar{c}}^2 m_{c\bar{q}}^2 \right\}. \quad (13)$$

The interchange of quarks brings about two scattering forms, the prior form and the post form. The two forms may lead to different values of the transition amplitude \mathcal{M}_{fi} (and the subsequent cross section), which is the so-called post-prior discrepancy [31–33]. Scattering in the prior form means that gluon exchange takes place prior to the quark interchange, and the corresponding transition amplitude is

$$\mathcal{M}_{\text{fi}}^{\text{prior}} = 4\sqrt{E_{q\bar{q}}E_{c\bar{c}}E_{q\bar{c}}E_{c\bar{q}}} < \psi_{q\bar{c}} | < \psi_{c\bar{q}} | (V_{q\bar{c}} + V_{c\bar{q}} + V_{qc} + V_{\bar{q}\bar{c}}) | \psi_{q\bar{q}} > | \psi_{c\bar{c}} >, \quad (14)$$

while scattering in the post form means that the quark interchange is followed by gluon exchange, and the corresponding transition amplitude is

$$\mathcal{M}_{\text{fi}}^{\text{post}} = 4\sqrt{E_{q\bar{q}}E_{c\bar{c}}E_{q\bar{c}}E_{c\bar{q}}} < \psi_{q\bar{c}} | < \psi_{c\bar{q}} | (V_{q\bar{q}} + V_{c\bar{c}} + V_{qc} + V_{\bar{q}\bar{c}}) | \psi_{q\bar{q}} > | \psi_{c\bar{c}} >, \quad (15)$$

where $\psi_{q\bar{c}}$ is the product of color, spin, flavor and momentum-space wave functions of the relative motion of q and \bar{c} and satisfies $\int \frac{d^3 p_{q\bar{c}}}{(2\pi)^3} \psi_{q\bar{c}}^+(\vec{p}_{q\bar{c}}) \psi_{q\bar{c}}(\vec{p}_{q\bar{c}}) = 1$ where $\vec{p}_{q\bar{c}}$ is the relative

momentum of q and \bar{c} , and similarly $\psi_{c\bar{q}}$, $\psi_{q\bar{q}}$ and $\psi_{c\bar{c}}$. A relative momentum depends on a linear combination of \vec{P} and \vec{P}' . The momentum-space wave functions are the Fourier transform of the coordinate-space wave functions which are solutions of the Schrödinger equation. In the transition amplitude we use the Fourier transform of the sum of the central spin-independent potential and the spin-spin interaction:

$$\begin{aligned}
V_{ab}(\vec{Q}) = & -\frac{\vec{\lambda}_a}{2} \cdot \frac{\vec{\lambda}_b}{2} \frac{3}{4} D \left[1.3 - \left(\frac{T}{T_c} \right)^4 \right] \left[(2\pi)^3 \delta^3(\vec{Q}) - \frac{8\pi}{Q} \int_0^\infty dr \frac{r \sin(Qr)}{\exp(2Ar) + 1} \right] \\
& + \frac{\vec{\lambda}_a}{2} \cdot \frac{\vec{\lambda}_b}{2} 64\pi E \int_0^\infty dq \frac{\rho(q^2) - \frac{K}{q^2}}{(E^2 + Q^2 + q^2)^2 - 4Q^2 q^2} \\
& - \frac{\vec{\lambda}_a}{2} \cdot \frac{\vec{\lambda}_b}{2} \frac{16\pi^2}{25} \frac{\vec{s}_a \cdot \vec{s}_b}{m_a m_b} + \frac{\vec{\lambda}_a}{2} \cdot \frac{\vec{\lambda}_b}{2} \frac{16\pi^2 \lambda}{25Q} \int_0^\infty dx \frac{d^2 v(x)}{dx^2} \sin\left(\frac{Q}{\lambda} x\right) \frac{\vec{s}_a \cdot \vec{s}_b}{m_a m_b}.
\end{aligned} \tag{16}$$

Let σ^{prior} and σ^{post} be the cross sections for scattering in the prior form and in the post form, respectively, and they are given by Eq. (11). The unpolarized cross section for $q\bar{q} + c\bar{c} \rightarrow q\bar{c} + c\bar{q}$ is

$$\begin{aligned}
\sigma^{\text{unpol}}(\sqrt{s}, T) = & \frac{1}{(2S_{q\bar{q}} + 1)(2S_{c\bar{c}} + 1)} \\
& \times \sum_S (2S + 1) \frac{\sigma^{\text{prior}}(S, m_S, \sqrt{s}, T) + \sigma^{\text{post}}(S, m_S, \sqrt{s}, T)}{2},
\end{aligned} \tag{17}$$

where $S_{q\bar{q}}$ and $S_{c\bar{c}}$ are the spins of $q\bar{q}$ and $c\bar{c}$, respectively.

4. Numerical cross sections and discussions

Quark-antiquark relative-motion wave functions of mesons are given by the Schrödinger equation with the central spin-independent potential V_{si} . With the up (down) quark mass 0.32 GeV and the experimental π mass, the experimental data of S -wave $I = 2$ elastic phase shifts for $\pi\pi$ scattering in vacuum [34–37] for $0 < \sqrt{s} < 2.4$ GeV are reproduced from the potential in Eq. (16) at $T = 0$ [20]. In the estimates of charmonium dissociation cross sections at $T = 0$, the experimental masses of pion, rho, charmonia, and charmed mesons are employed. For $0.6 < T/T_c < 1$ we use the temperature-dependent meson

masses shown in Fig. 1 and the π and ρ masses in Fig. 2 of Ref. [20]. Temperature dependence of charmonium dissociation cross sections shown in the next subsection seems to be complicated, but is understandable.

From $T = 0.6T_c$ to $0.99T_c$ the masses of π , ρ , J/ψ , ψ' , χ_c , D , and D^* are reduced by 0.40955 GeV, 0.60936 GeV, 0.21908 GeV, 0.56022 GeV, 0.53639 GeV, 0.35318 GeV, and 0.53845 GeV, respectively. The reduced amounts of ψ' , χ_c and D^* masses are between the ones of π and ρ masses. Hence, the difference $m_{q\bar{c}} + m_{c\bar{q}} - m_{q\bar{q}} - m_{c\bar{c}}$ may be larger or smaller than zero. Whether a reaction is endothermic or not depends on temperature. A reaction may be exothermic below a temperature and endothermic above the temperature.

4.1. Numerical cross sections

The temperature-dependent potential given in Eq. (16), the wave functions, and the meson masses in the transition amplitude make both the meson-charmonium dissociation cross sections and relevant threshold energies dependent on temperature. In Figs. 2-16 we plot cross sections for the following fifteen meson-charmonium dissociation reactions: $\pi J/\psi \rightarrow \bar{D}^* D$ or $\bar{D} D^*$, $\pi J/\psi \rightarrow \bar{D}^* D^*$, $\pi \psi' \rightarrow \bar{D}^* D$ or $\bar{D} D^*$, $\pi \psi' \rightarrow \bar{D}^* D^*$, $\pi \chi_c \rightarrow \bar{D}^* D$ or $\bar{D} D^*$, $\pi \chi_c \rightarrow \bar{D}^* D^*$, $\rho J/\psi \rightarrow \bar{D} D$, $\rho J/\psi \rightarrow \bar{D}^* D$ or $\bar{D} D^*$, $\rho J/\psi \rightarrow \bar{D}^* D^*$, $\rho \psi' \rightarrow \bar{D} D$, $\rho \psi' \rightarrow \bar{D}^* D$ or $\bar{D} D^*$, $\rho \psi' \rightarrow \bar{D}^* D^*$, $\rho \chi_c \rightarrow \bar{D} D$, $\rho \chi_c \rightarrow \bar{D}^* D$ or $\bar{D} D^*$, and $\rho \chi_c \rightarrow \bar{D}^* D^*$. Here D stands for D^+ or D^0 , \bar{D} for D^- or \bar{D}^0 , D^* for D^{*+} or D^{*0} , and \bar{D}^* for D^{*-} or \bar{D}^{*0} . For the reaction that produces $\bar{D}^* D$ or $\bar{D} D^*$, the cross section for the production of $\bar{D} D^*$ equals the one of $\bar{D}^* D$. No matter what the temperature is, the reactions, $\pi J/\psi \rightarrow \bar{D}^* D$, $\pi J/\psi \rightarrow \bar{D}^* D^*$, $\pi \psi' \rightarrow \bar{D}^* D^*$, $\pi \chi_c \rightarrow \bar{D}^* D^*$, $\rho J/\psi \rightarrow \bar{D}^* D$, and $\rho J/\psi \rightarrow \bar{D}^* D^*$, are endothermic. No reactions are all exothermic from $T = 0.6T_c$ to T_c . To display in-medium modification of dissociation, we plot the cross sections at $T = 0$ for reference even though they differ from the results obtained in Ref. [18] from the potential that includes the color Coulomb, spin-spin hyperfine and linear confinement terms.

4.2. Endothermic reactions of $\pi \psi'$, $\pi \chi_c$, $\rho \psi'$ and $\rho \chi_c$

The cross sections for endothermic $\pi\psi'$ and $\pi\chi_c$ reactions in Figs. 4-7 show that peak cross sections increase from $T/T_c = 0$ to 0.75 and decrease from $T/T_c = 0.75$ to 0.95 except the increasing peak cross section from $T/T_c = 0.9$ to 0.95 in Fig. 5 for $\pi\psi' \rightarrow \bar{D}^*D^*$. While temperature increases from zero, the large-distance potential given by the first term in Eq. (1) becomes smaller and smaller, and the Schrödinger equation with the potential shown by Eq. (1) produces increasing meson radius. The increase of initial-meson radii leads to peak cross sections increasing from $T/T_c = 0$ to 0.75. With increasing temperature, it becomes more difficult to combine the interchanged quarks and the antiquarks to form mesons $q\bar{c}$ and $c\bar{q}$ due to weakening confinement. This leads to peak cross sections decreasing from $T/T_c = 0.75$ to 0.95. This also explains the decrease of the peak cross section from $T/T_c = 0.85$ to 0.9 in Fig. 13 for $\rho\psi' \rightarrow \bar{D}^*D^*$, from $T/T_c = 0.9$ to 0.95 in Fig. 11 for $\rho\psi' \rightarrow \bar{D}D$, Fig. 12 for $\rho\psi' \rightarrow \bar{D}^*D$, Fig. 14 for $\rho\chi_c \rightarrow \bar{D}D$ and Fig. 15 for $\rho\chi_c \rightarrow \bar{D}^*D$, or from $T/T_c = 0.85$ to 0.95 in Fig. 16 for $\rho\chi_c \rightarrow \bar{D}^*D^*$.

We have already known that ψ' and χ_c have very similar temperature dependence in mass. The $\pi\psi'$ ($\rho\psi'$) and $\pi\chi_c$ ($\rho\chi_c$) reactions are almost identical in threshold energy, but are different in cross section even though the final mesons in the $\pi\psi'$ ($\rho\psi'$) reactions are the same as those in the $\pi\chi_c$ ($\rho\chi_c$) reactions. The difference is clearly attributed to the different quantum numbers of ψ' and χ_c . Particularly, when T/T_c goes from 0.9 to 0.95, the increase of the peak cross section of $\pi\psi' \rightarrow \bar{D}^*D^*$ in Fig. 5 ($\rho\psi' \rightarrow \bar{D}^*D^*$ in Fig. 13) is against the decrease of the peak cross section of $\pi\chi_c \rightarrow \bar{D}^*D^*$ in Fig. 7 ($\rho\chi_c \rightarrow \bar{D}^*D^*$ in Fig. 16). This relates to the node in the ψ' wave function. The node leads to cancellation between the negative wave function on the left of the node and the positive wave function on the right of the node in the integration involved in the transition amplitude. While the cancellation at $T = 0.95T_c$ is less than at $T = 0.9T_c$, the peak cross sections of $\pi\psi' \rightarrow \bar{D}^*D^*$ and $\rho\psi' \rightarrow \bar{D}^*D^*$ rise from $T/T_c = 0.9$ to 0.95.

4.3. Exothermic reactions of $\pi\psi'$, $\pi\chi_c$, $\rho\psi'$, $\rho\chi_c$ and $\rho J/\psi$

Since cross sections for exothermic reactions at threshold energies are infinite, we start

calculating the cross sections at $\sqrt{s} = m_{q\bar{q}} + m_{c\bar{c}} + \Delta\sqrt{s}$ with $\Delta\sqrt{s} = 10^{-4}$ GeV. At the energies the cross sections correspond to the curve tops, for example, the top of the curve for $T/T_c = 0.65$ displayed in Fig. 4, and from Eq. (12) we have

$$\vec{P}^2 \approx 2 \Delta \sqrt{s} / \left(\frac{1}{m_{q\bar{q}}} + \frac{1}{m_{c\bar{c}}} \right), \quad (18)$$

which indicates that \vec{P}^2 decreases with decreasing meson mass. In Section 2 we have obtained that the meson masses decrease with increasing temperature. Hence, $|\vec{P}|$ decreases while temperature increases. At $T = 0.6T_c$, $|\vec{P}|$ is estimated at about 10^{-2} GeV. The influence of \vec{P} on the relative momenta \vec{p}_{ab} is thus negligible. Finally, \vec{p}_{ab} is governed by \vec{P}' that obeys

$$m_{q\bar{q}} + m_{c\bar{c}} + \Delta\sqrt{s} = \sqrt{m_{q\bar{c}}^2 + \vec{P}'^2} + \sqrt{m_{c\bar{q}}^2 + \vec{P}'^2}. \quad (19)$$

Since $\Delta\sqrt{s}$ is very small, we have

$$\vec{P}'^2 \approx 2(m_{q\bar{q}} + m_{c\bar{c}} - m_{q\bar{c}} - m_{c\bar{q}}) / \left(\frac{1}{m_{q\bar{c}}} + \frac{1}{m_{c\bar{q}}} \right). \quad (20)$$

With increasing temperature the value of $m_{q\bar{q}} + m_{c\bar{c}} - m_{q\bar{c}} - m_{c\bar{q}}$ decreases in the region where reactions are exothermic, and becomes zero at a temperature; meanwhile, $|\vec{P}'|$ decreases so that the absolute value of the relative-motion part of $\psi_{ab}(\vec{p}_{ab})$ gets larger and larger, and the factor $\sqrt{E_{q\bar{q}}E_{c\bar{c}}E_{q\bar{c}}E_{c\bar{q}}}$ in the transition amplitude decreases. Simple calculations show that the factor $\frac{1}{s} \frac{|\vec{P}'|}{|\vec{P}|}$ generally decreases with increasing temperature in the region where reactions are exothermic. The product of the increasing absolute value of the relative-motion part of $\psi_{ab}(\vec{p}_{ab})$ and the decreasing $\frac{1}{s} \frac{|\vec{P}'|}{|\vec{P}|} E_{q\bar{q}}E_{c\bar{c}}E_{q\bar{c}}E_{c\bar{q}}$ leads to that the cross section at $\sqrt{s} = m_{q\bar{q}} + m_{c\bar{c}} + \Delta\sqrt{s}$ first increases and then decreases as shown in Figs. 6, 8, and 16, or first decreases and then increases in Figs. 4 and 11 through 15.

4.4. Endothermic reactions of $\pi J/\psi$ and $\rho J/\psi$

As shown in Figs. 2-3 and 8-10, the peak cross sections of the endothermic $\pi J/\psi$ and $\rho J/\psi$ reactions decrease from $T = 0$ to $0.85T_c$ and increase from $T = 0.85T_c$ to $0.95T_c$. The behavior of the peak cross sections is different from that of the endothermic reaction $\pi\chi_c \rightarrow \bar{D}^*D^*$, which is an increase from $T = 0$ to $0.75T_c$ and a decrease from $T = 0.75T_c$

to $0.95T_c$. The behavior must come from a special point, and as demonstrated below, the special point is just the temperature dependence of the mass and radius of J/ψ .

First, we discuss cross sections for $\pi J/\psi$ and $\rho J/\psi$ dissociation in the region $0 \leq T/T_c \leq 0.85$. In Section 2 we have obtained the slow decrease of ψ' , χ_c and D^* masses and the very slow decrease of J/ψ and D masses when T/T_c increases from 0 to 0.85. It is shown in Fig. 2 of Ref. [20] that the π mass decreases slowly for $0.6T_c \leq T < 0.78T_c$ and the ρ mass does rapidly. Then, $\frac{1}{s} \frac{|\vec{P}'|}{|\vec{P}|}$ keeps roughly unchanged or decreases. Since the J/ψ radius changes very slowly in comparison to the increase of the π or ρ radius, only one increasing initial-meson radius causes the increase of $|\mathcal{M}_{\text{fi}}|^2$, and the increase can not overcome the amount reduced by the weakening confinement with increasing temperature, i.e. $|\mathcal{M}_{\text{fi}}|^2$ decreases. Finally, the product of $\frac{1}{s} \frac{|\vec{P}'|}{|\vec{P}|}$ and $|\mathcal{M}_{\text{fi}}|^2$ leads to the decrease of the peak cross sections of the endothermic $\pi J/\psi$ and $\rho J/\psi$ reactions when T/T_c increases from 0 to 0.85.

Next, we discuss cross sections for $\pi J/\psi$ and $\rho J/\psi$ dissociation in the region $0.85 \leq T/T_c < 1$. The factor $\frac{1}{s} \frac{|\vec{P}'|}{|\vec{P}|}$ increases by about 50% from $T = 0.85T_c$ to $0.9T_c$ and by about 100% from $T = 0.9T_c$ to $0.95T_c$. When temperature increases from $T = 0.85T_c$ to $0.95T_c$, not only the π and ρ radii increase, but also the J/ψ radius apparently does. Now the increase of $|\mathcal{M}_{\text{fi}}|^2$ caused by the increasing radii of the two initial mesons overcomes the amount reduced by the weakening confinement with increasing temperature. Finally, the peak cross sections of the endothermic $\pi J/\psi$ and $\rho J/\psi$ reactions increase from $T/T_c = 0.85$ to 0.95 .

4.5. Comparison of π + charmonium reactions and ρ + charmonium reactions

We make a comparison of peak cross sections of endothermic π + charmonium reactions with ones of endothermic ρ + charmonium reactions. We find that the peak cross section of $\pi J/\psi \rightarrow \bar{D}^* D$ ($\pi \chi_c \rightarrow \bar{D}^* D$) is larger than that of $\rho J/\psi \rightarrow \bar{D}^* D$ ($\rho \chi_c \rightarrow \bar{D}^* D$) at the same temperature while the peak cross section of π + charmonium $\rightarrow \bar{D}^* + D^*$ ($\pi \psi' \rightarrow \bar{D}^* D$) is smaller than the one of ρ + charmonium $\rightarrow \bar{D}^* + D^*$ ($\rho \psi' \rightarrow \bar{D}^* D$). Exothermic π + charmonium reactions and exothermic ρ + charmonium reactions are

compared about their cross sections at $\sqrt{s} = m_{q\bar{q}} + m_{c\bar{c}} + 10^{-4}$ GeV (the largest cross section shown in each curve). It is shown in Figs. 4, 6, 12 and 15 that the cross section of $\pi + \text{charmonium} \rightarrow \bar{D}^* + D$ at $T/T_c = 0.65$ or 0.75 is larger than the one of $\rho + \text{charmonium} \rightarrow \bar{D}^* + D$ at the same temperature. It is meaningless to compare endothermic $\pi + \text{charmonium}$ reactions (e.g. $\pi\psi' \rightarrow \bar{D}^*D$ at $T/T_c = 0.85$) with exothermic $\rho + \text{charmonium}$ reactions (e.g. $\rho\psi' \rightarrow \bar{D}^*D$ at the same temperature).

Regarding endothermic reactions we examine \vec{P} and \vec{P}' at $\sqrt{s} = m_{q\bar{c}} + m_{c\bar{q}} + d_0$ at which the peak cross sections are given and $d_0 \ll m_{q\bar{c}} + m_{c\bar{q}}$. Eq. (13) yields

$$\vec{P}'^2 \approx 2d_0 / \left(\frac{1}{m_{q\bar{c}}} + \frac{1}{m_{c\bar{q}}} \right). \quad (21)$$

From an endothermic $\pi + \text{charmonium}$ reaction to an endothermic $\rho + \text{charmonium}$ reaction at the same temperature, $m_{q\bar{c}}$ and $m_{c\bar{q}}$ do not change, and d_0 decreases or does not change. Accordingly, \vec{P}'^2 is reduced or unchanged. \sqrt{s} is related to initial-meson energies by

$$m_{q\bar{c}} + m_{c\bar{q}} + d_0 = \sqrt{m_{q\bar{q}}^2 + \vec{P}^2} + \sqrt{m_{c\bar{c}}^2 + \vec{P}^2}, \quad (22)$$

which let \vec{P}^2 decrease from the endothermic $\pi + \text{charmonium}$ reaction to the endothermic $\rho + \text{charmonium}$ reaction. As a result the absolute value of the relative-motion part of $\psi_{ab}(\vec{p}_{ab})$ in the transition amplitude increases.

In the transition amplitude ψ_{ab} is the product of color, spin, flavor and momentum-space wave functions of the relative motion of constituents a and b . The transition amplitude involves the spin factor: the matrix elements of $\vec{s}_a \cdot \vec{s}_b$ of the spin-spin interaction and the overlap of the spin wave function of final mesons and the one of initial mesons. The difference of the transition amplitudes for $\pi + \text{charmonium} \rightarrow \bar{D}^* + D$ and for $\rho + \text{charmonium} \rightarrow \bar{D}^* + D$ is caused by not only the difference of the π and ρ masses (the subsequent changes of $\sqrt{E_{q\bar{q}}E_{c\bar{c}}E_{q\bar{c}}E_{c\bar{q}}}$, $\psi_{ab}(\vec{p}_{ab})$, and $|\vec{P}'|/s|\vec{P}|$) but also the difference of the spin factors for the two reactions. Particularly, π and ρ become almost degenerate in mass at $T/T_c \geq 0.9$. Then, only the spin factors made the peak cross section of $\pi + \text{charmonium} \rightarrow \bar{D}^* + D$ larger or smaller than the one of $\rho + \text{charmonium} \rightarrow \bar{D}^* + D$. In case the final mesons are \bar{D}^* and D^* , the total spin of π and charmonium is 1 that

differs from the total spins 0, 1 and 2 of ρ and charmonium. The spin factors plus the additional contribution of the channels of the total spins 0 and 2 of ρ and charmonium make the peak cross section of $\pi + \text{charmonium} \rightarrow \bar{D}^* + D^*$ smaller than the one of $\rho + \text{charmonium} \rightarrow \bar{D}^* + D^*$ at $T/T_c = 0.9$ and 0.95 . The difference between the cross sections at $\sqrt{s} = m_{q\bar{q}} + m_{c\bar{c}} + 10^{-4}$ GeV for exothermic $\pi + \text{charmonium} \rightarrow \bar{D}^* + D$ and for exothermic $\rho + \text{charmonium} \rightarrow \bar{D}^* + D$ can be understood similarly with Eqs. (18) and (19).

5. Results pertinent to smearing in the spin-spin interaction

We have solved the Schrödinger equation with the central spin-independent potential V_{si} in Section 2. If we use the spin-spin interaction given in Eq. (3) in the Schrödinger equation, the delta function in the first term of the V_{ss} expression cannot be correctly dealt with. However, in the present section we take smearing in the spin-spin interaction by the regularization $\delta^3(\vec{r}) \rightarrow \frac{d^3}{\pi^{3/2}} \exp(-d^2 r^2)$, and the smeared spin-spin interaction

$$V_{\text{ss}} = -\frac{\vec{\lambda}_a}{2} \cdot \frac{\vec{\lambda}_b}{2} \frac{16\pi^2}{25} \frac{d^3}{\pi^{3/2}} \exp(-d^2 r^2) \frac{\vec{s}_a \cdot \vec{s}_b}{m_a m_b} + \frac{\vec{\lambda}_a}{2} \cdot \frac{\vec{\lambda}_b}{2} \frac{4\pi}{25} \frac{1}{r} \frac{d^2 v(\lambda r)}{dr^2} \frac{\vec{s}_a \cdot \vec{s}_b}{m_a m_b}, \quad (23)$$

can be used in the Schrödinger equation. Such smearing actually includes relativistic effects [17, 19, 38]. The quantity d is related to quark masses by

$$d^2 = \sigma_0^2 \left[\frac{1}{2} + \frac{1}{2} \left(\frac{4m_a m_b}{(m_a + m_b)^2} \right)^4 \right] + \sigma_1^2 \left(\frac{2m_a m_b}{m_a + m_b} \right)^2,$$

where $\sigma_0 = 0.15$ GeV and $\sigma_1 = 0.705$. By solving the Schrödinger equation with the central spin-independent potential and the smeared spin-spin interaction, we obtain meson masses and quark-antiquark relative-motion wave functions that differ by different mesons. The ρ wave function is near that obtained by the Schrödinger equation with only V_{si} , but the π wave function is not. Since the smeared spin-spin interaction is used, the pion becomes a tight bound state of a quark and an antiquark. Then, the π radius increases slowly from 0.6 to 0.9 of T/T_c and quickly from 0.9 to 1 of T/T_c .

The mass splittings at $T = 0$ are $m_\rho - m_\pi = 0.6294$ GeV and $m_{K^*} - m_K = 0.39865$ GeV which are closer to the experimental data 0.6304 GeV and 0.3963 GeV than the results

(0.5989 GeV and 0.3833 GeV) [20] of the Schrödinger equation with only the central spin-independent potential. At $T=0$ we also get 3.13509 GeV, 3.69248 GeV, 3.50578 GeV, 1.90578 GeV, 2.05274 GeV, 1.9614 GeV, and 2.13804 GeV as the masses of J/ψ , ψ' , χ_c , D , D^* , D_s , and D_s^* , respectively, compared to the measured values 3.096916 GeV, 3.68609 GeV, 3.5253 GeV, 1.86722 GeV, 2.00861 GeV, 1.96847 GeV, and 2.1123 GeV [28]. For $0.6 \leq T/T_c < 1$ temperature dependence of the ρ , K^* , J/ψ , ψ' , χ_c , D , D^* , D_s and D_s^* masses obtained with the potential $V_{\text{si}} + V_{\text{ss}}$ is very close to that obtained with only V_{si} . Therefore, the parametrizations given in Eqs. (4)-(10) are also valid in the present section, and the ρ and K^* masses in units of GeV in the region $0.6 \leq T/T_c < 1$ are parametrized as

$$m_\rho = 0.73 \left[1 - \left(\frac{T}{0.992T_c} \right)^{3.67} \right]^{0.989}, \quad (24)$$

$$m_{K^*} = 0.84 \left[1 - \left(\frac{T}{1.05T_c} \right)^{4.16} \right]. \quad (25)$$

However, the π , K and η masses obtained with $V_{\text{si}} + V_{\text{ss}}$ are smaller than those obtained with only V_{si} . They are plotted in Fig. 17 for $0.6 \leq T/T_c < 1$ and are parametrized as

$$m_\pi = 0.24 \left[1 - \left(\frac{T}{0.97T_c} \right)^{3.81} \right]^{0.51}, \quad (26)$$

$$m_K = 0.46 \left[1 - \left(\frac{T}{1.04T_c} \right)^{8.58} \right]^{0.88}, \quad (27)$$

$$m_\eta = 0.55 \left[1 - \left(\frac{T}{1.01T_c} \right)^{3.11} \right]^{0.29}, \quad (28)$$

in units of GeV.

Corresponding to the π mass, the reactions $\pi J/\psi \rightarrow \bar{D}^* D$, $\pi J/\psi \rightarrow \bar{D}^* D^*$, $\pi \psi' \rightarrow \bar{D}^* D$, $\pi \psi' \rightarrow \bar{D}^* D^*$, $\pi \chi_c \rightarrow \bar{D}^* D$, and $\pi \chi_c \rightarrow \bar{D}^* D^*$ are all endothermic. Cross sections for the reactions are calculated with the experimental meson masses at $T = 0$, the temperature-dependent meson masses for $0.6 \leq T/T_c < 1$, the quark-antiquark relative-motion wave functions and the Fourier transform of the sum of the central spin-

independent potential and the smeared spin-spin interaction

$$\begin{aligned}
V_{ab}(\vec{Q}) = & -\frac{\vec{\lambda}_a}{2} \cdot \frac{\vec{\lambda}_b}{2} \frac{3}{4} D \left[1.3 - \left(\frac{T}{T_c} \right)^4 \right] \left[(2\pi)^3 \delta^3(\vec{Q}) - \frac{8\pi}{Q} \int_0^\infty dr \frac{r \sin(Qr)}{\exp(2Ar) + 1} \right] \\
& + \frac{\vec{\lambda}_a}{2} \cdot \frac{\vec{\lambda}_b}{2} 64\pi E \int_0^\infty dq \frac{\rho(q^2) - \frac{K}{q^2}}{(E^2 + Q^2 + q^2)^2 - 4Q^2 q^2} \\
& - \frac{\vec{\lambda}_a}{2} \cdot \frac{\vec{\lambda}_b}{2} \frac{16\pi^2}{25} \exp\left(-\frac{Q^2}{4d^2}\right) \frac{\vec{s}_a \cdot \vec{s}_b}{m_a m_b} \\
& + \frac{\vec{\lambda}_a}{2} \cdot \frac{\vec{\lambda}_b}{2} \frac{16\pi^2 \lambda}{25Q} \int_0^\infty dx \frac{d^2 v(x)}{dx^2} \sin\left(\frac{Q}{\lambda} x\right) \frac{\vec{s}_a \cdot \vec{s}_b}{m_a m_b}.
\end{aligned} \tag{29}$$

We plot the cross sections for the reactions in Figs. 18-23. The cross sections differ from those shown in Figs. 2-7. For example, the reactions $\pi\psi' \rightarrow \bar{D}^* D$ and $\pi\chi_c \rightarrow \bar{D}^* D$ at $T/T_c = 0.65$ and 0.75 are exothermic in Figs. 4 and 6 but endothermic in Figs. 20 and 22. One feature for each reaction is that the peak cross section at $T/T_c = 0.95$ is always larger than the ones at the other five temperatures $T/T_c = 0, 0.65, 0.75, 0.85, 0.9$. This is caused by the π and J/ψ radii which increase faster from 0.9 to 1 of T/T_c than from 0.6 to 0.9 of T/T_c . The numerical cross sections for endothermic reactions are parametrized as

$$\begin{aligned}
\sigma^{\text{unpol}}(\sqrt{s}, T) = & a_1 \left(\frac{\sqrt{s} - \sqrt{s_0}}{b_1} \right)^{c_1} \exp \left[c_1 \left(1 - \frac{\sqrt{s} - \sqrt{s_0}}{b_1} \right) \right] \\
& + a_2 \left(\frac{\sqrt{s} - \sqrt{s_0}}{b_2} \right)^{c_2} \exp \left[c_2 \left(1 - \frac{\sqrt{s} - \sqrt{s_0}}{b_2} \right) \right],
\end{aligned} \tag{30}$$

where $\sqrt{s_0}$ is the threshold energy, and a_1, b_1, c_1, a_2, b_2 and c_2 are parameters. Determination of parameter values needs time-consuming computations, and the values are listed in Tables 1-3.

Since the $\rho, J/\psi, \psi', \chi_c, D$ and D^* masses determined by the Schrödinger equation in the case of $V_{\text{si}} + V_{\text{ss}}$ are very close to the masses determined by the Schrödinger equation in the case of only V_{si} , a ρ -charmonium dissociation reaction which is endothermic (exothermic) in the former case is also endothermic (exothermic) in the latter case, and $\frac{1}{s} \frac{|\vec{P}'|}{|\vec{P}|}$ in the two cases are quite close. Since \sqrt{s} dependence of the cross section for a quark-interchange-induced reaction is mainly determined by $\frac{1}{s} \frac{|\vec{P}'|}{|\vec{P}|}$ [30], \sqrt{s} dependence of

the cross section for a ρ -charmonium reaction in the former case is similar to one in the latter case. Hence, we do not plot ρ -charmonium dissociation cross sections in the case of $V_{\text{si}} + V_{\text{ss}}$, but present parametrizations of these cross sections. The cross section for the exothermic reaction $q\bar{q}(S_{q\bar{q}}; \vec{P}) + c\bar{c}(S_{c\bar{c}}; -\vec{P}) \rightarrow q\bar{c}(S_{q\bar{c}}; \vec{P}') + c\bar{q}(S_{c\bar{q}}; -\vec{P}')$ can be related to the endothermic reaction $q\bar{c} + c\bar{q} \rightarrow q\bar{q} + c\bar{c}$ by the detailed balance

$$\sigma_{q\bar{q}+c\bar{c} \rightarrow q\bar{c}+c\bar{q}}^{\text{unpol}} = \frac{(2S_{q\bar{c}}+1)(2S_{c\bar{q}}+1)}{(2S_{q\bar{q}}+1)(2S_{c\bar{c}}+1)} \frac{\vec{P}'^2}{\vec{P}^2} \sigma_{q\bar{c}+c\bar{q} \rightarrow q\bar{q}+c\bar{c}}^{\text{unpol}}, \quad (31)$$

where $S_{q\bar{c}}$ and $S_{c\bar{q}}$ are the spins of $q\bar{c}$ and $c\bar{q}$, respectively. It is then correct to choose the following parametrization for the exothermic reaction

$$\begin{aligned} \sigma^{\text{unpol}}(\sqrt{s}, T) = & \frac{\vec{P}'^2}{\vec{P}^2} \left\{ a_1 \left(\frac{\sqrt{s} - \sqrt{s_0}}{b_1} \right)^{c_1} \exp \left[c_1 \left(1 - \frac{\sqrt{s} - \sqrt{s_0}}{b_1} \right) \right] \right. \\ & \left. + a_2 \left(\frac{\sqrt{s} - \sqrt{s_0}}{b_2} \right)^{c_2} \exp \left[c_2 \left(1 - \frac{\sqrt{s} - \sqrt{s_0}}{b_2} \right) \right] \right\}. \end{aligned} \quad (32)$$

Parameter values are listed in Tables 4-6.

6. Procedure

The curves shown in Figs. 2-16 and 18-23 correspond to the zero temperature and the five nonzero temperatures $T_1 = 0.65T_c$, $T_2 = 0.75T_c$, $T_3 = 0.85T_c$, $T_4 = 0.9T_c$ and $T_5 = 0.95T_c$. We now present a procedure on how to obtain the unpolarized cross section for $q\bar{q} + c\bar{c} \rightarrow q\bar{c} + c\bar{q}$ for $0.65T_c \leq T < T_c$ from the curves.

First, we state the procedure while a reaction at T_i and T_{i+1} is endothermic. We denote by $\sqrt{s_p}$ the square root of the Mandelstam variable corresponding to the peak cross section. $d_0 = \sqrt{s_p} - \sqrt{s_0}$ is the difference of $\sqrt{s_p}$ with respect to the threshold energy $\sqrt{s_0}$. Let $\sqrt{s_z}$ be the square root of the Mandelstam variable at which the cross section is 1/100 of the peak cross section, and $\sqrt{s_z} > \sqrt{s_p} > \sqrt{s_0}$. d_0 , $\sqrt{s_z}$, $\sqrt{s_0}$, and $\sqrt{s_p}$ at T_i are indicated by d_{0i} , $\sqrt{s_{zi}}$, $\sqrt{s_{0i}}$, and $\sqrt{s_{pi}}$, respectively. d_{0i} and $\sqrt{s_{zi}}$ can be found in Tables 1-6. $\sqrt{s_{0i}}$ can be obtained from the mass parametrizations in Section 2, and $\sqrt{s_{pi}} = \sqrt{s_{0i}} + d_{0i}$. For $T_i \leq T \leq T_{i+1}$ ($i=1, 2, 3$ or 4) we take the linear interpolation between the two peaks at T_i and T_{i+1} to estimate d_0 and $\sqrt{s_z}$ of the cross section at T ,

$$d_0 = \frac{d_{0i+1} - d_{0i}}{T_{i+1} - T_i} (T - T_i) + d_{0i}, \quad (33)$$

$$\sqrt{s_z} = \frac{\sqrt{s_{zi+1}} - \sqrt{s_{zi}}}{T_{i+1} - T_i}(T - T_i) + \sqrt{s_{zi}}. \quad (34)$$

$\sqrt{s_0}$ is the sum of final-meson masses, and parametrizations of the masses have been given by Eqs. (7) and (8). The square root of the Mandelstam variable corresponding to the peak cross section is $\sqrt{s_p} = \sqrt{s_0} + d_0$. We define a ratio

$$\zeta = \begin{cases} \frac{\sqrt{s} - \sqrt{s_p}}{\sqrt{s_0} - \sqrt{s_p}} & \text{if } \sqrt{s_0} \leq \sqrt{s} \leq \sqrt{s_p} \\ \frac{\sqrt{s} - \sqrt{s_p}}{\sqrt{s_z} - \sqrt{s_p}} & \text{if } \sqrt{s_p} < \sqrt{s} \leq \sqrt{s_z}. \end{cases} \quad (35)$$

The ratio ζ is on the closed interval $[0,1]$, and corresponds to \sqrt{s} and T . In the cross section curve at T_i , we can find a point $(\sqrt{s_i}, \sigma_i^{\text{unpol}}(\sqrt{s_i}, T_i))$ which gives the same ratio,

$$\zeta = \begin{cases} \frac{\sqrt{s_i} - \sqrt{s_{pi}}}{\sqrt{s_{0i}} - \sqrt{s_{pi}}} & \text{if } \sqrt{s_{0i}} \leq \sqrt{s_i} \leq \sqrt{s_{pi}} \\ \frac{\sqrt{s_i} - \sqrt{s_{pi}}}{\sqrt{s_{zi}} - \sqrt{s_{pi}}} & \text{if } \sqrt{s_{pi}} < \sqrt{s_i} \leq \sqrt{s_{zi}}, \end{cases} \quad (36)$$

and in the cross section curve at T_{i+1} , we find a point $(\sqrt{s_{i+1}}, \sigma_{i+1}^{\text{unpol}}(\sqrt{s_{i+1}}, T_{i+1}))$ which also gives the ratio

$$\zeta = \begin{cases} \frac{\sqrt{s_{i+1}} - \sqrt{s_{pi+1}}}{\sqrt{s_{0i+1}} - \sqrt{s_{pi+1}}} & \text{if } \sqrt{s_{0i+1}} \leq \sqrt{s_{i+1}} \leq \sqrt{s_{pi+1}} \\ \frac{\sqrt{s_{i+1}} - \sqrt{s_{pi+1}}}{\sqrt{s_{zi+1}} - \sqrt{s_{pi+1}}} & \text{if } \sqrt{s_{pi+1}} < \sqrt{s_{i+1}} \leq \sqrt{s_{zi+1}}. \end{cases} \quad (37)$$

The regions $\sqrt{s_{0i}} \leq \sqrt{s_i} \leq \sqrt{s_{pi}}$ and $\sqrt{s_{0i+1}} \leq \sqrt{s_{i+1}} \leq \sqrt{s_{pi+1}}$ ($\sqrt{s_{pi}} < \sqrt{s_i} \leq \sqrt{s_{zi}}$ and $\sqrt{s_{pi+1}} < \sqrt{s_{i+1}} \leq \sqrt{s_{zi+1}}$) correspond to $\sqrt{s_0} \leq \sqrt{s} \leq \sqrt{s_p}$ ($\sqrt{s_p} < \sqrt{s} \leq \sqrt{s_z}$). In terms of the ratio $\sqrt{s_i}$ and $\sqrt{s_{i+1}}$ are expressed as

$$\sqrt{s_i} = \begin{cases} \sqrt{s_{pi}} + \zeta(\sqrt{s_{0i}} - \sqrt{s_{pi}}) & \text{if } \sqrt{s_0} \leq \sqrt{s} \leq \sqrt{s_p} \\ \sqrt{s_{pi}} + \zeta(\sqrt{s_{zi}} - \sqrt{s_{pi}}) & \text{if } \sqrt{s_p} < \sqrt{s} \leq \sqrt{s_z}, \end{cases} \quad (38)$$

$$\sqrt{s_{i+1}} = \begin{cases} \sqrt{s_{pi+1}} + \zeta(\sqrt{s_{0i+1}} - \sqrt{s_{pi+1}}) & \text{if } \sqrt{s_0} \leq \sqrt{s} \leq \sqrt{s_p} \\ \sqrt{s_{pi+1}} + \zeta(\sqrt{s_{zi+1}} - \sqrt{s_{pi+1}}) & \text{if } \sqrt{s_p} < \sqrt{s} \leq \sqrt{s_z}. \end{cases} \quad (39)$$

The linear interpolation between the two points provides the unpolarized cross section at \sqrt{s} for $T_i \leq T \leq T_{i+1}$,

$$\sigma^{\text{unpol}}(\sqrt{s}, T) = \begin{cases} \frac{\sigma_{i+1}^{\text{unpol}}(\sqrt{s_{i+1}}, T_{i+1}) - \sigma_i^{\text{unpol}}(\sqrt{s_i}, T_i)}{T_{i+1} - T_i}(T - T_i) + \sigma_i^{\text{unpol}}(\sqrt{s_i}, T_i) & \text{if } \sqrt{s_0} \leq \sqrt{s} \leq \sqrt{s_z} \\ 0 & \text{if } \sqrt{s} > \sqrt{s_z}. \end{cases} \quad (40)$$

where σ_i^{unpol} and $\sigma_{i+1}^{\text{unpol}}$ are shown in Figs. 2-16 and 18-23, and are given by Eq. (30) together with the parameters listed in Tables 1-6. For $0.95T_c < T < T_c$ Eqs. (33)-(40) still apply to obtaining the unpolarized cross section so long as $T_i = T_4$ and $T_{i+1} = T_5$ are set.

Second, we state the procedure while a reaction at T_i and T_{i+1} is exothermic. Eqs. (33)-(40) are suited to endothermic reactions of which each has the zero cross section at the threshold energy or at the infinite total energy of initial mesons and has one maximum cross section in its \sqrt{s} dependence. The cross section for the exothermic reaction is infinite at the threshold energy. But the quantity enclosed by the braces in Eq. (32) has the general \sqrt{s} dependence of endothermic reactions. Hence, Eqs. (33)-(39) apply to the quantity enclosed by the braces. d_{0i} and $\sqrt{s_{zi}}$ of the quantity are listed in Tables 4-6. $\sqrt{s_0}$ equals the sum of initial-meson masses, and parametrizations of the masses have been given by Eqs. (4), (5), (6), and (24). Eq. (40) now gives the unpolarized cross section for the exothermic reaction at T while σ_i^{unpol} and $\sigma_{i+1}^{\text{unpol}}$ are the cross sections shown in Figs. 8 and 11-16, and are given by Eq. (32) together with the parameters listed in Tables 4-6. Since the infinity of the cross section at the threshold energy is intractable, do not let \sqrt{s} equal $\sqrt{s_0}$ while fortran code is made.

Third, we state the procedure while a reaction is exothermic at T_i and endothermic at T_{i+1} . Eqs. (33)-(39) apply to the endothermic reaction at T_{i+1} or the quantity enclosed by the braces in Eq. (32) at T_i . Relevant d_{0i} , $\sqrt{s_{zi}}$, d_{0i+1} , and $\sqrt{s_{zi+1}}$ can be found in Tables 4-6. $\sqrt{s_{0i}}$ and $\sqrt{s_{0i+1}}$ equal the sum of initial-meson masses and the sum of final-meson masses, respectively. $\sqrt{s_0}$ at T is the sum of final-meson masses for $m_{q\bar{c}} + m_{c\bar{q}} - m_{q\bar{q}} - m_{c\bar{c}} > 0$ or the sum of initial-meson masses for $m_{q\bar{c}} + m_{c\bar{q}} - m_{q\bar{q}} - m_{c\bar{c}} < 0$. After estimating $\sqrt{s_i}$ and $\sqrt{s_{i+1}}$, Eq. (40) is used to get the unpolarized cross section at \sqrt{s} for $T_i \leq T \leq T_{i+1}$ while $\sigma_i^{\text{unpol}}(\sqrt{s_i}, T_i)$ is the cross section for the exothermic reaction and $\sigma_{i+1}^{\text{unpol}}(\sqrt{s_{i+1}}, T_{i+1})$ for the endothermic reaction.

7. Summary

The central spin-independent and temperature-dependent potential has been used in

the Schrödinger equation to obtain the temperature-dependent masses of J/ψ , ψ' , χ_c , D , D^* , D_s and D_s^* as well as the wave functions of quark-antiquark relative motion inside these mesons. The experimental masses of the mesons are reproduced by the potential at $T = 0$. While temperature increases, the temperature dependence of the theoretical masses is: the ψ' and χ_c masses decrease slowly, and the J/ψ mass more slowly; each of the D and D_s masses keeps almost unchanged in a temperature region, and apparently falls off near T_c ; the D^* and D_s^* masses first decrease slowly, and then apparently fall off. The prominent medium effects are: ψ' and χ_c are degenerate in mass for $0.6T_c < T < T_c$; very near the critical temperature J/ψ , ψ' , and χ_c become a mass triplet, and D and D^* (D_s and D_s^*) become degenerate in mass. These are also true when the central spin-independent potential and the smeared spin-spin interaction are used in the Schrödinger equation to obtain temperature-dependent masses and quark-antiquark relative-motion wave functions. The particular temperature dependence of the J/ψ mass and radius causes the peak cross sections of the endothermic $\pi J/\psi$ and $\rho J/\psi$ reactions to increase rapidly when temperature approaches the critical temperature. Even though ψ' and χ_c are degenerate in mass, the cross sections of ψ' and χ_c in collisions with a light meson are different, which is owed to the node of the ψ' wave function. The temperature dependence of the potential, the quark-antiquark relative-motion wave functions, and the meson masses leads to the temperature dependence of all dissociation cross sections by the three factors, the difference $m_{q\bar{c}} + m_{c\bar{q}} - m_{q\bar{q}} - m_{c\bar{c}}$, $\frac{1}{s} \frac{|\vec{P}'|}{|\vec{P}|}$, and the transition amplitude. Some reactions are purely endothermic while the others become exothermic below certain temperatures. Parametrizations of unpolarized cross sections are given for $\pi J/\psi \rightarrow \bar{D}^* D$ or $\bar{D} D^*$, $\pi J/\psi \rightarrow \bar{D}^* D^*$, $\pi \psi' \rightarrow \bar{D}^* D$ or $\bar{D} D^*$, $\pi \psi' \rightarrow \bar{D}^* D^*$, $\pi \chi_c \rightarrow \bar{D}^* D$ or $\bar{D} D^*$, $\pi \chi_c \rightarrow \bar{D}^* D^*$, $\rho J/\psi \rightarrow \bar{D} D$, $\rho J/\psi \rightarrow \bar{D}^* D$ or $\bar{D} D^*$, $\rho J/\psi \rightarrow \bar{D}^* D^*$, $\rho \psi' \rightarrow \bar{D} D$, $\rho \psi' \rightarrow \bar{D}^* D$ or $\bar{D} D^*$, $\rho \psi' \rightarrow \bar{D}^* D^*$, $\rho \chi_c \rightarrow \bar{D} D$, $\rho \chi_c \rightarrow \bar{D}^* D$ or $\bar{D} D^*$, and $\rho \chi_c \rightarrow \bar{D}^* D^*$. The parametrizations at the five temperatures, $T/T_c = 0.65, 0.75, 0.85, 0.9, 0.95$, can be used in the procedure to yield cross sections at any temperature between $0.65T_c$ and T_c .

Acknowledgements

This work was supported by the National Natural Science Foundation of China under Grant No. 11175111.

References

- [1] T. Matsui and H. Satz, Phys. Lett. B 178, 416 (1986).
- [2] J. Schukraft, Talk presented at the 22nd International Conference on Ultra-Relativistic Nucleus-Nucleus Collisions, Annecy, France, May 23-28, 2011.
- [3] B. Wyslouch, Talk presented at the 22nd International Conference on Ultra-Relativistic Nucleus-Nucleus Collisions, Annecy, France, May 23-28, 2011.
- [4] J. Ftáčnik, P. Lichard, and J. Pišút, Phys. Lett. B 207, 194 (1988); S. Gavin, M. Gyulassy, and A. Jackson, Phys. Lett. B 207, 257 (1988); R. Vogt, M. Prakash, P. Koch, and T. H. Hansson, Phys. Lett. B 207, 263 (1988); C. Gerschel and J. Hüfner, Phys. Lett. B 207, 253 (1988).
- [5] M. E. Peskin, Nucl. Phys. B 156, 365 (1979); G. Bhanot and M. E. Peskin, Nucl. Phys. B 156, 391 (1979).
- [6] D. Kharzeev and H. Satz, Phys. Lett. B 334, 155 (1994).
- [7] F. Arleo, P. B. Gossiaux, T. Gousset, and J. Aichelin, Phys. Rev. D 65, 014005 (2001).
- [8] S. G. Matinyan and B. Müller, Phys. Rev. C 58, 2994 (1998).
- [9] Z. Lin and C. M. Ko, Phys. Rev. C 62, 034903 (2000); J. Phys. G 27, 617 (2001).
- [10] K. L. Haglin, Phys. Rev. C 61, 031902 (2000); K. L. Haglin and C. Gale, Phys. Rev. C 63, 065201 (2001).
- [11] Y. Oh, T. Song, and S. H. Lee, Phys. Rev. C 63, 034901 (2001).
- [12] F. S. Navarra, M. Nielsen, and M. R. Robilotta, Phys. Rev. C 64, 021901(R) (2001).
- [13] L. Maiani, F. Piccinini, A. D. Polosa, and V. Riquer, Nucl. Phys. A 741, 273 (2004).
- [14] A. Bourque and C. Gale, Phys. Rev. C 78, 035206 (2008); Phys. Rev. C 80, 015204 (2009).
- [15] K. Martins, D. Blaschke, and E. Quack, Phys. Rev. C 51, 2723 (1995).
- [16] C.-Y. Wong, E. S. Swanson, and T. Barnes, Phys. Rev. C 62, 045201 (2000).
- [17] C.-Y. Wong, E. S. Swanson, and T. Barnes, Phys. Rev. C 65, 014903 (2001).

- [18] T. Barnes, E. S. Swanson, C.-Y. Wong, and X.-M. Xu, Phys. Rev. C 68, 014903 (2003).
- [19] T. Barnes and E. S. Swanson, Phys. Rev. D 46, 131 (1992); E. S. Swanson, Ann. Phys. (N.Y.) 220, 73 (1992).
- [20] Y.-P. Zhang, X.-M. Xu, and H.-J. Ge, Nucl. Phys. A 832, 112 (2010).
- [21] A. De Rújula, H. Georgi, and S. L. Glashow, Phys. Rev. D 12, 147 (1975).
- [22] N. Isgur and G. Karl, Phys. Rev. D 18, 4187 (1978); Phys. Rev. D 19, 2653 (1979); Phys. Rev. D 20, 1191 (1979).
- [23] S. Godfrey and N. Isgur, Phys. Rev. D 32, 189 (1985).
- [24] S. Capstick and N. Isgur, Phys. Rev. D 34, 2809 (1986).
- [25] F. Karsch, E. Laermann, and A. Peikert, Nucl. Phys. B 605, 579 (2001).
- [26] W. Buchmüller and S.-H. H. Tye, Phys. Rev. D 24, 132 (1981).
- [27] E. Eichten *et al.*, Phys. Rev. D 17, 3090 (1978); Phys. Rev. D 21, 203 (1980).
- [28] K. Nakamura *et al.* (Particle Data Group), J. Phys. G 37, 075021 (2010).
- [29] X.-M. Xu, Nucl. Phys. A 697, 825 (2002).
- [30] Y.-Q. Li and X.-M. Xu, Nucl. Phys. A 794, 210 (2007).
- [31] N. F. Mott and H. S. W. Massey, The Theory of Atomic Collisions, Clarendon Press, Oxford, 1965.
- [32] T. Barnes, N. Black, and E. S. Swanson, Phys. Rev. C 63, 025204 (2001).
- [33] C.-Y. Wong and H. W. Crater, Phys. Rev. C 63, 044907 (2001).
- [34] E. Colton *et al.*, Phys. Rev. D 3, 2028 (1971).
- [35] N. B. Durusoy *et al.*, Phys. Lett. B 45, 517 (1973).
- [36] W. Hoogland *et al.*, Nucl. Phys. B 126, 109 (1977).
- [37] M. J. Losty *et al.*, Nucl. Phys. B 69, 185 (1974).
- [38] C.-Y. Wong, Phys. Rev. C 65, 034902 (2002).

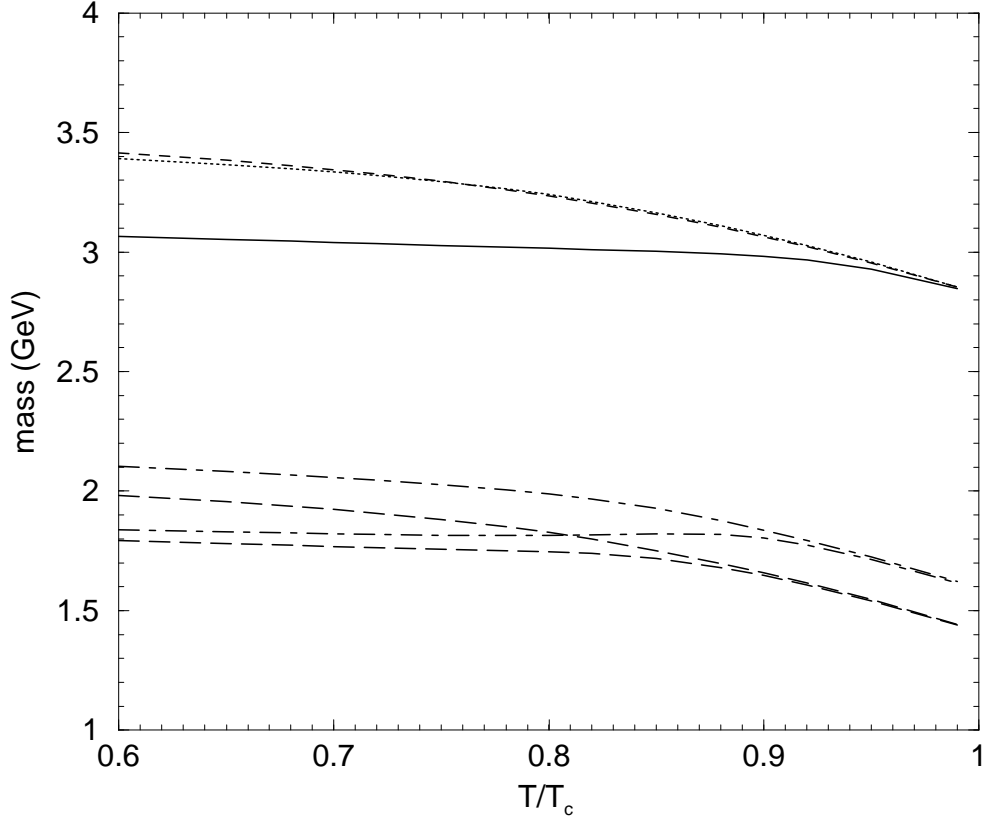


Figure 1: Meson masses as functions of T/T_c . The masses of J/ψ , ψ' , χ_c , D , D^* , D_s and D_s^* are shown by the solid, dashed, dotted, lower long dashed, upper long dashed, lower dot-dashed and upper dot-dashed curves, respectively.

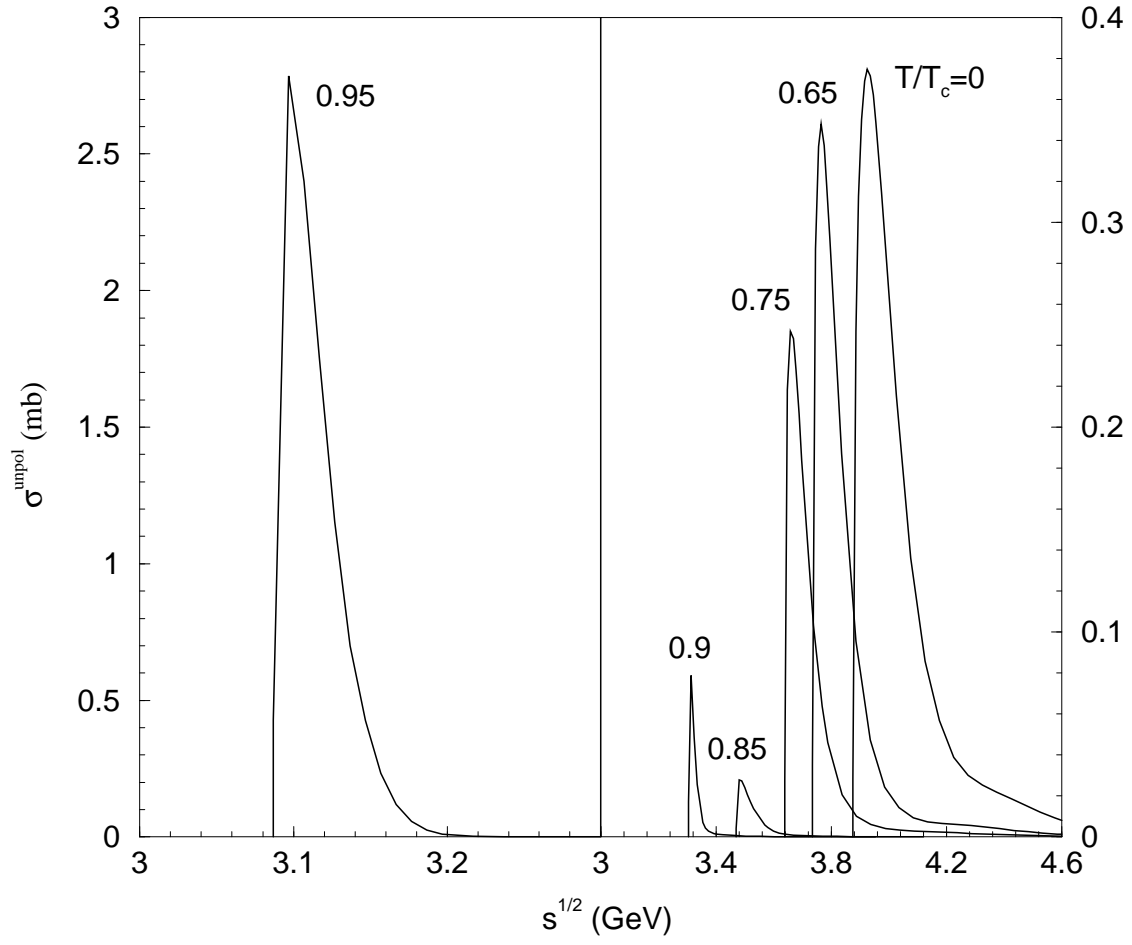


Figure 2: Cross sections for $\pi J/\psi \rightarrow \bar{D}^* D$ or $\bar{D} D^*$ at various temperatures.

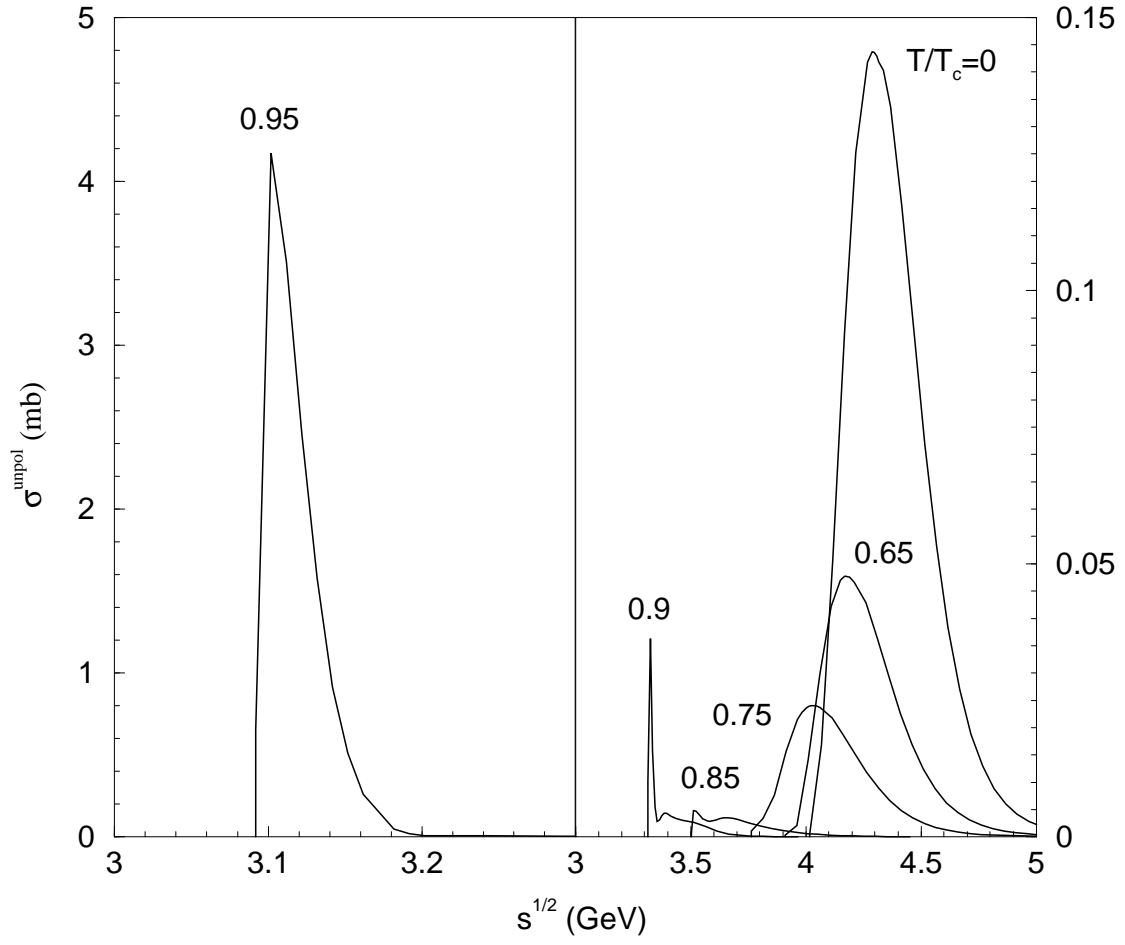


Figure 3: Cross sections for $\pi J/\psi \rightarrow \bar{D}^* D^*$ at various temperatures.

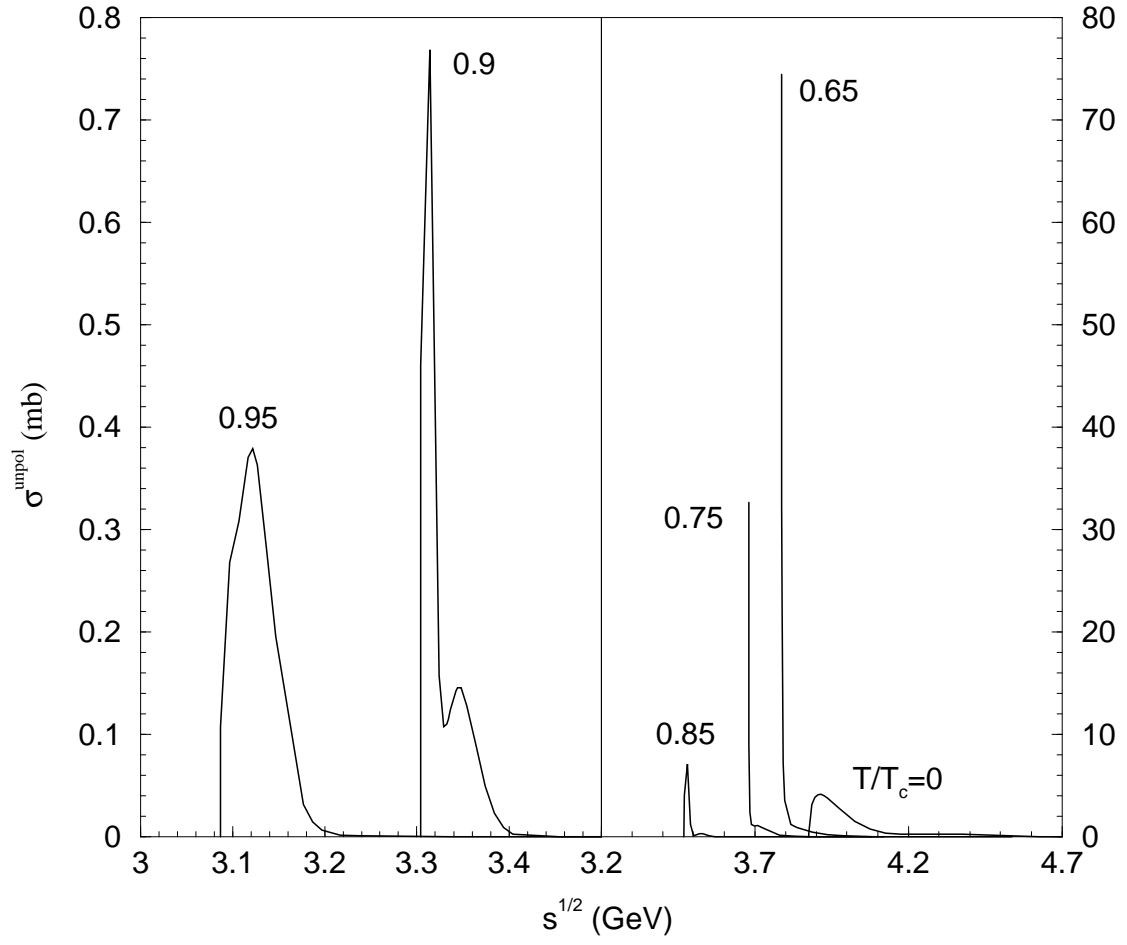


Figure 4: Cross sections for $\pi\psi' \rightarrow \bar{D}^*D$ or $\bar{D}D^*$ at various temperatures.

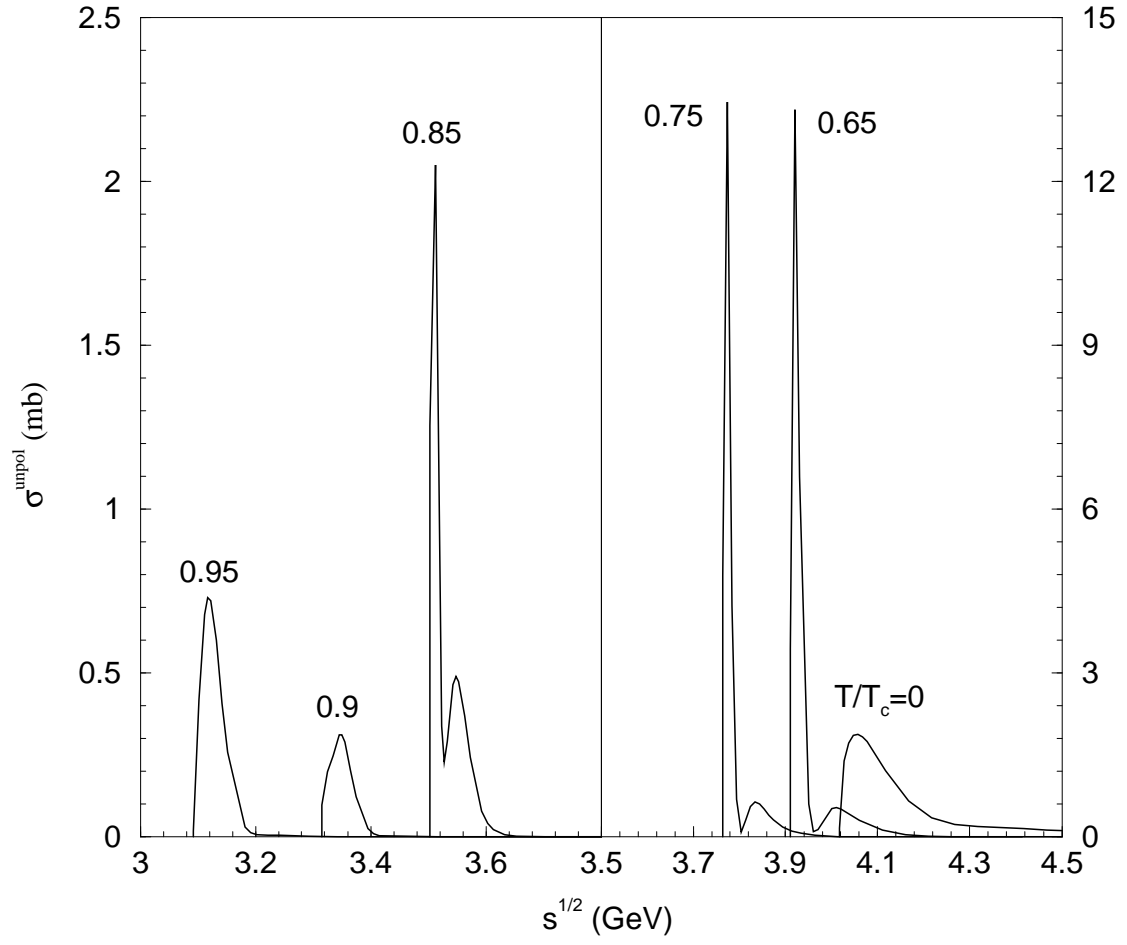


Figure 5: Cross sections for $\pi\psi' \rightarrow \bar{D}^*D^*$ at various temperatures.

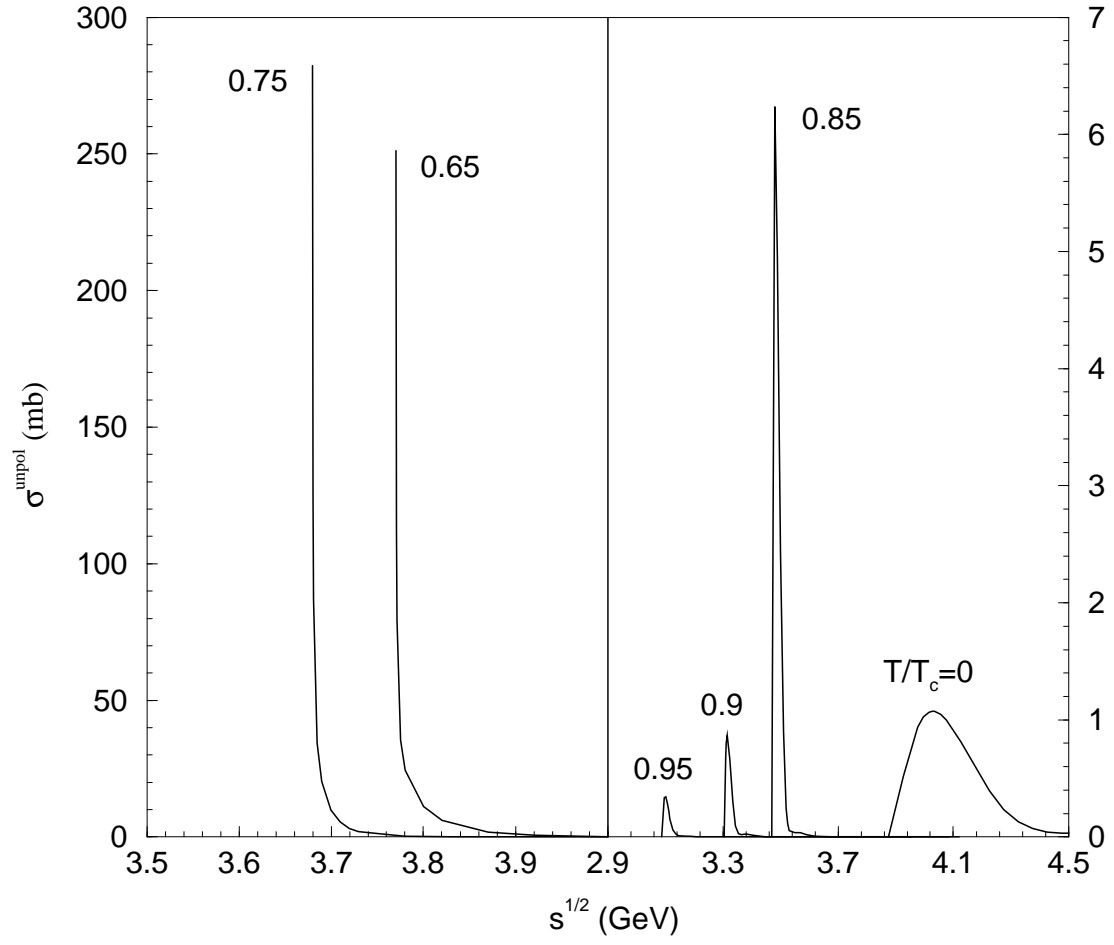


Figure 6: Cross sections for $\pi\chi_c \rightarrow \bar{D}^*D$ or $\bar{D}D^*$ at various temperatures.

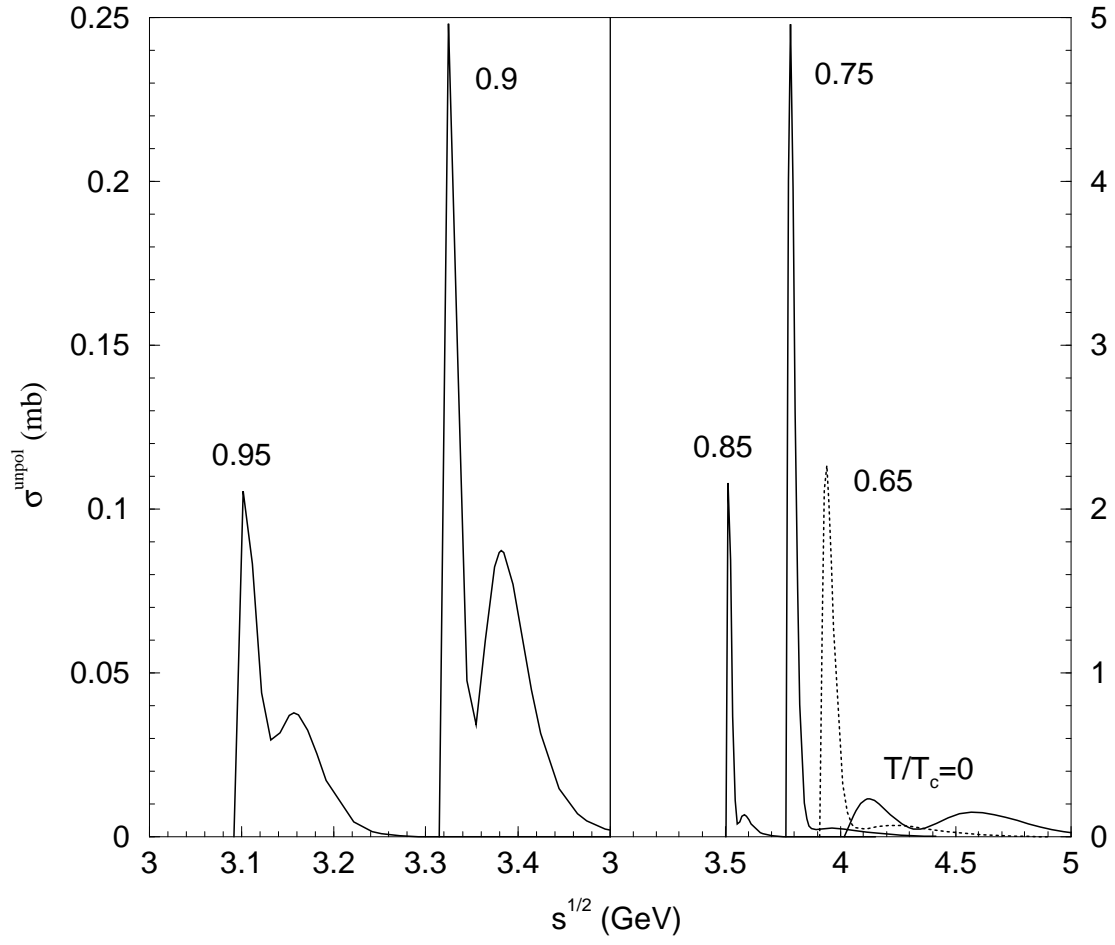


Figure 7: Cross sections for $\pi\chi_c \rightarrow \bar{D}^* D^*$ at various temperatures.

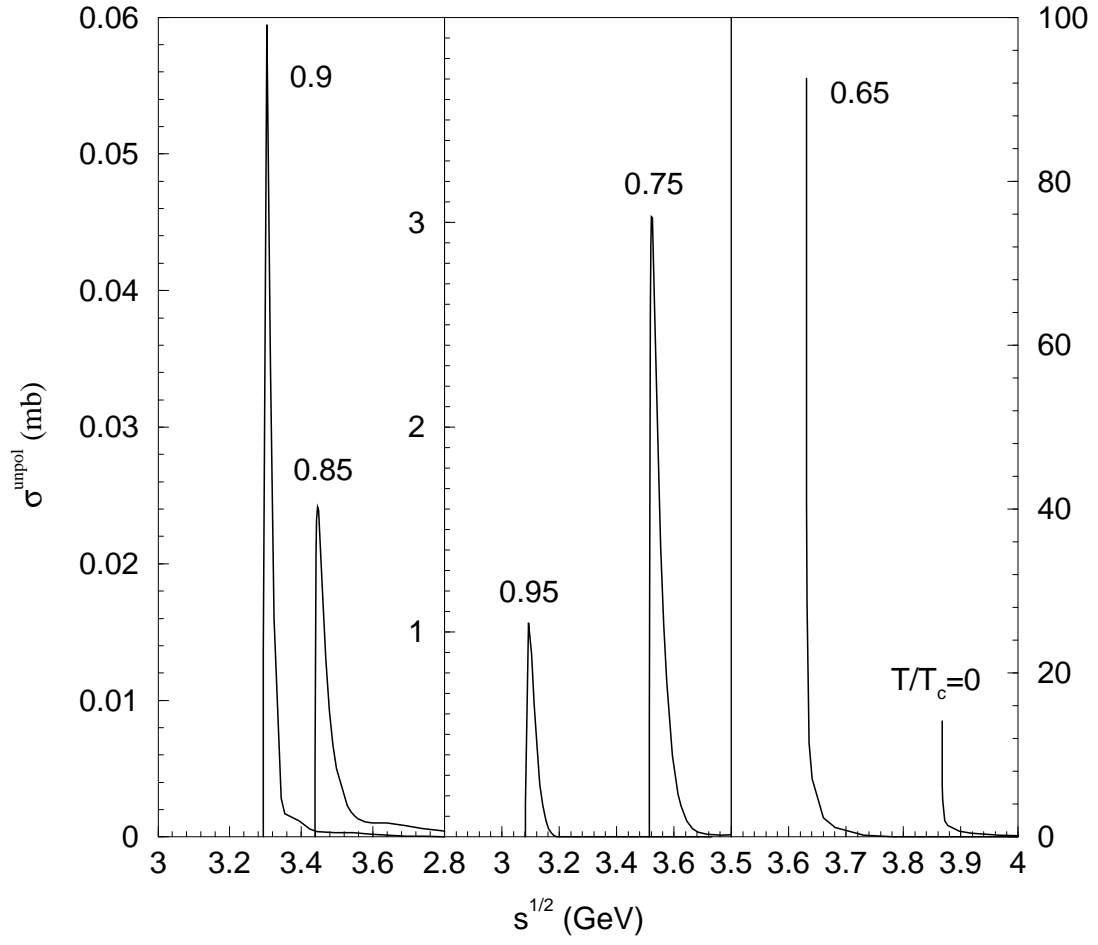


Figure 8: Cross sections for $\rho J/\psi \rightarrow \bar{D}D$ at various temperatures.

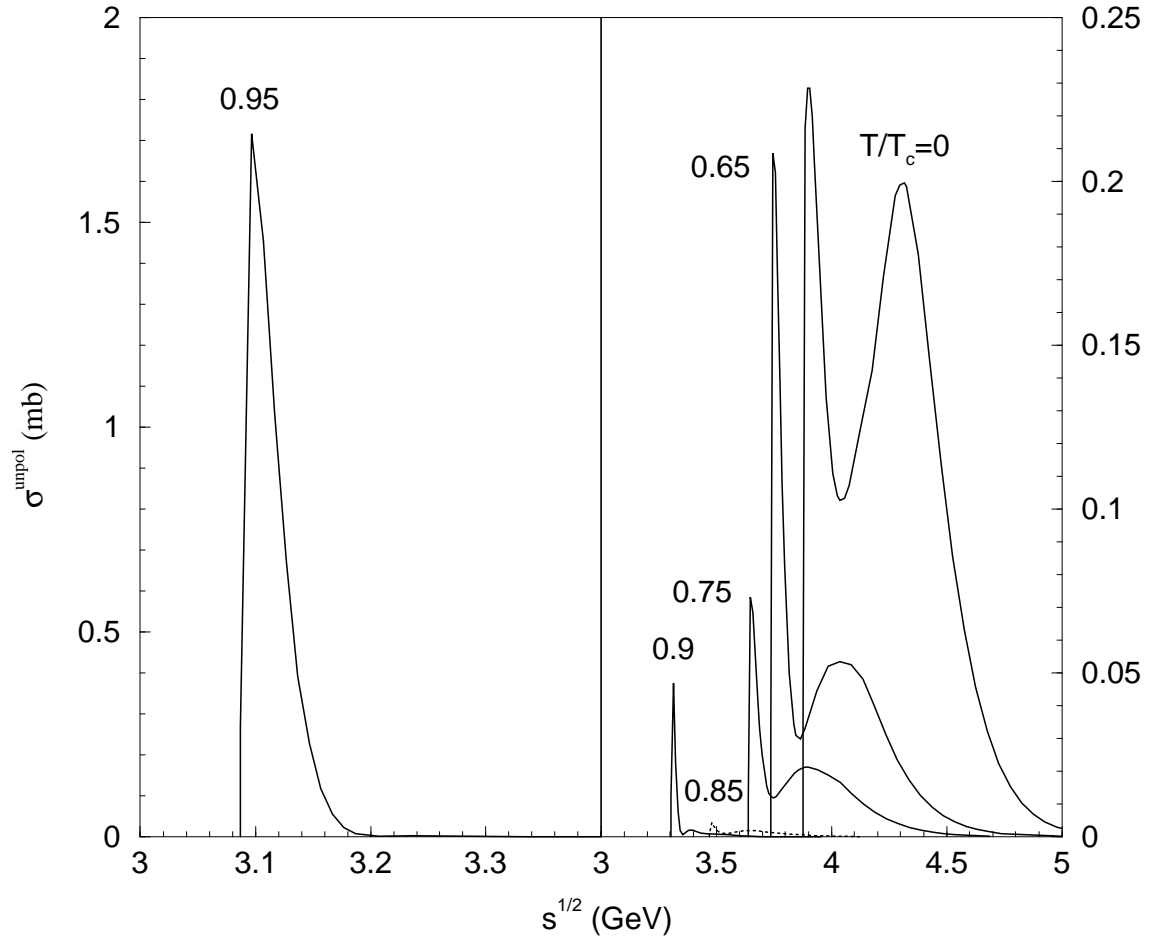


Figure 9: Cross sections for $\rho J/\psi \rightarrow \bar{D}^* D$ or $\bar{D} D^*$ at various temperatures.

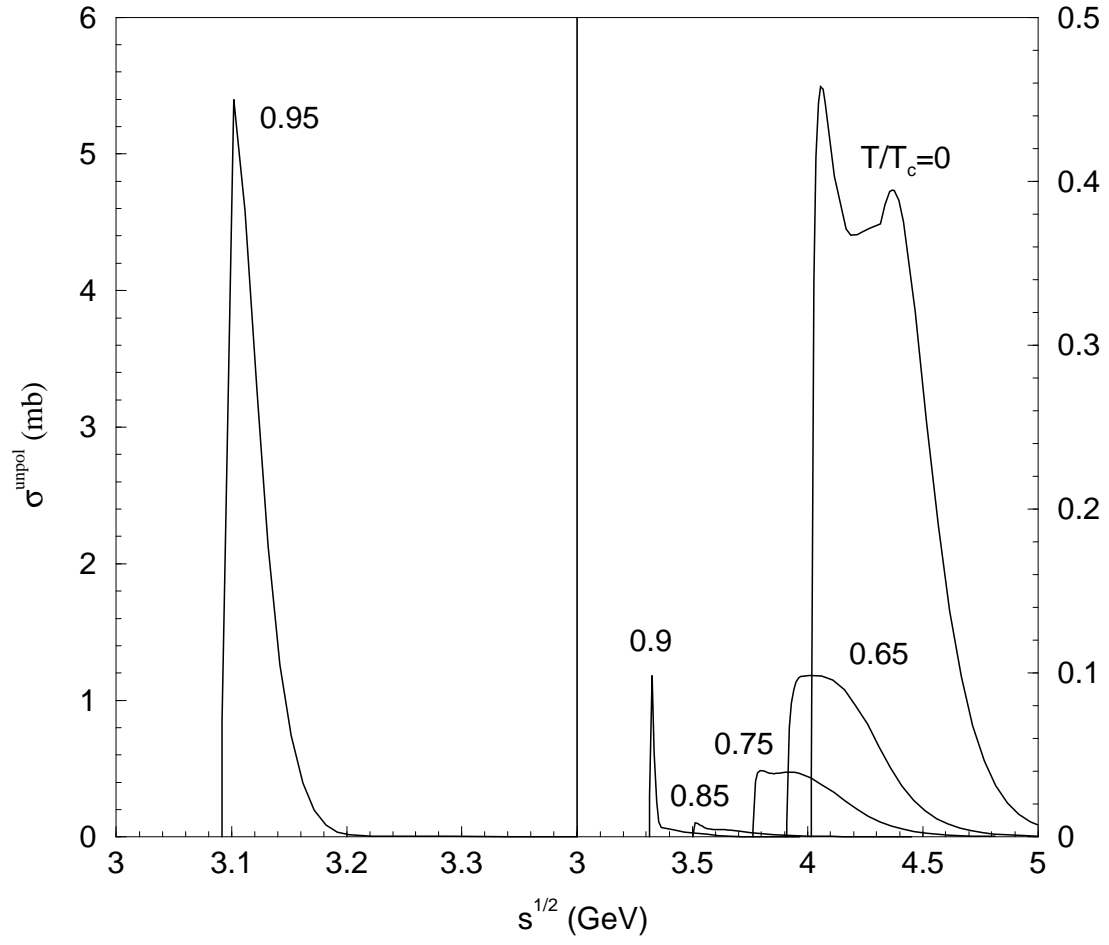


Figure 10: Cross sections for $\rho J/\psi \rightarrow \bar{D}^* D^*$ at various temperatures.

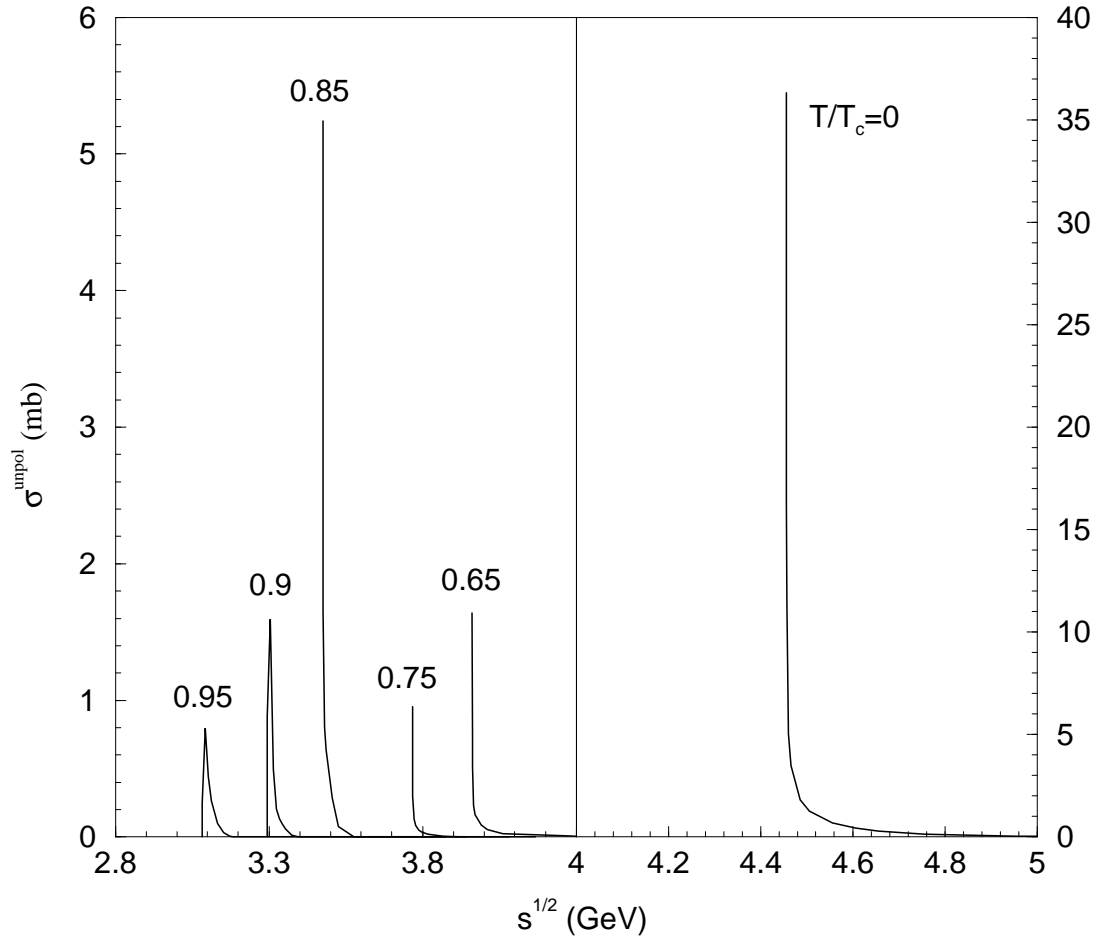


Figure 11: Cross sections for $\rho\psi' \rightarrow \bar{D}D$ at various temperatures.

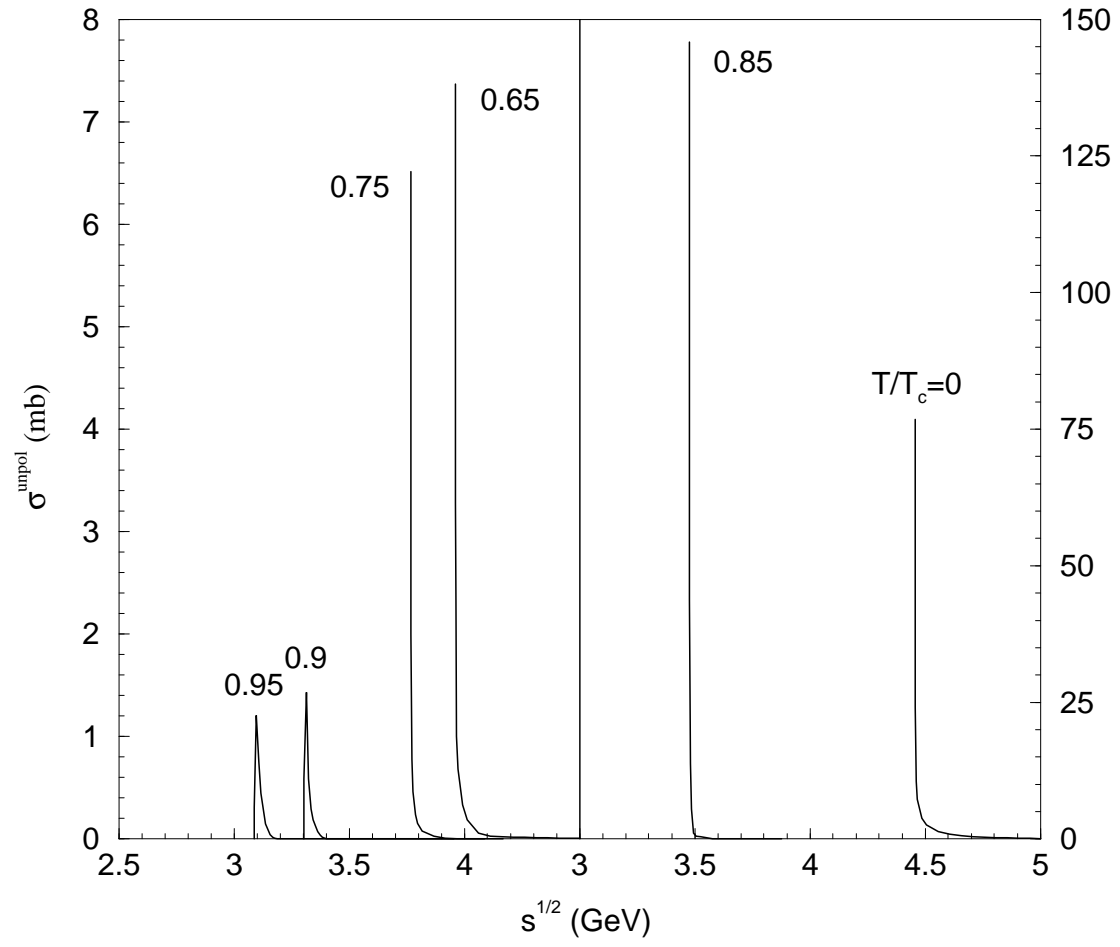


Figure 12: Cross sections for $\rho\psi' \rightarrow \bar{D}^*D$ or $\bar{D}D^*$ at various temperatures.

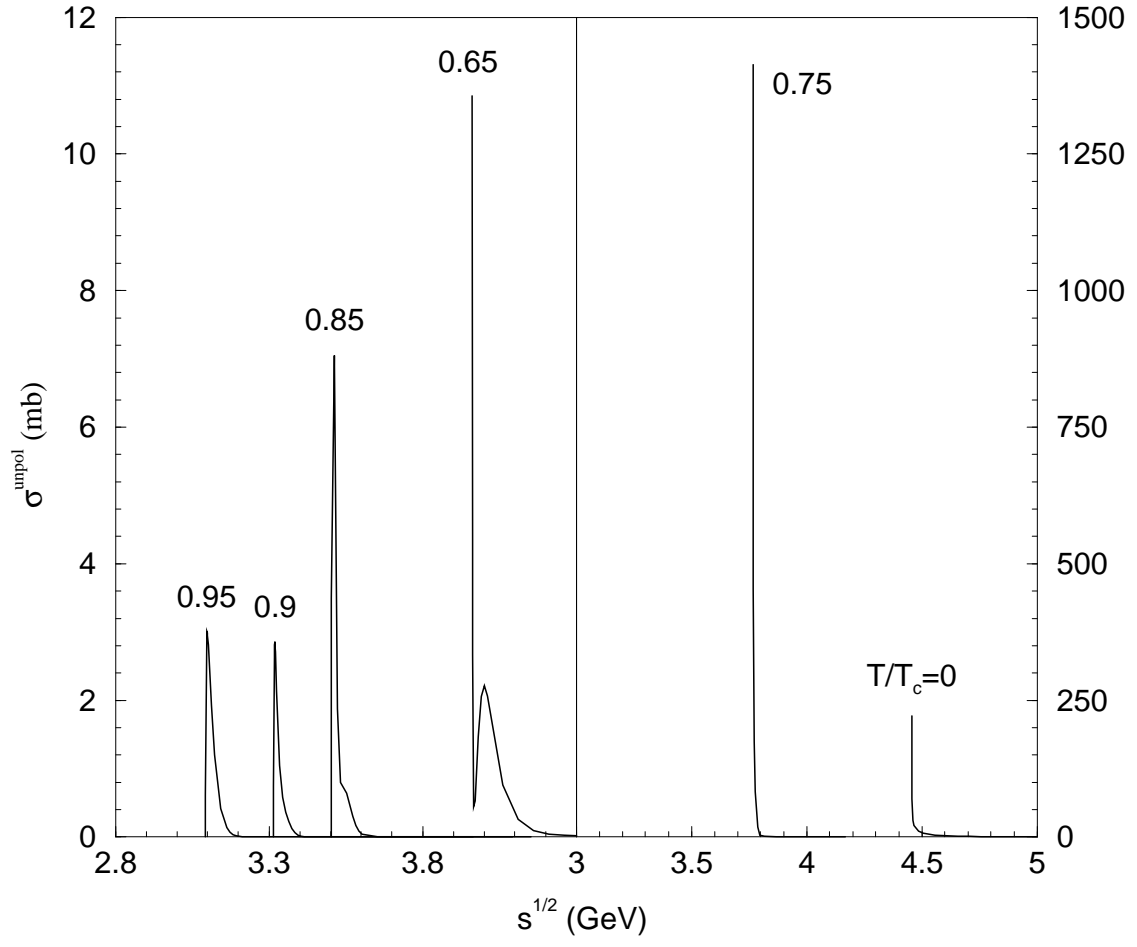


Figure 13: Cross sections for $\rho\psi' \rightarrow \bar{D}^*D^*$ at various temperatures.

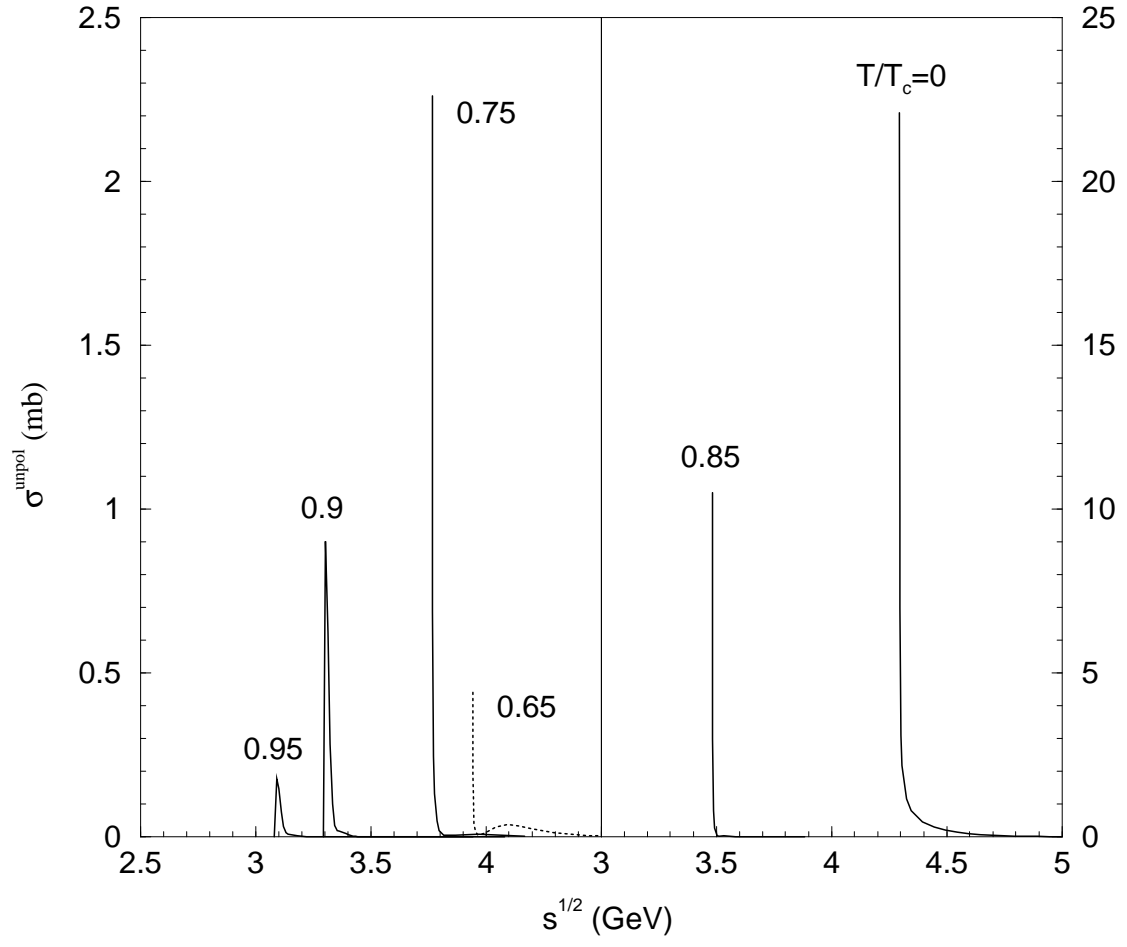


Figure 14: Cross sections for $\rho\chi_c \rightarrow \bar{D}D$ at various temperatures.

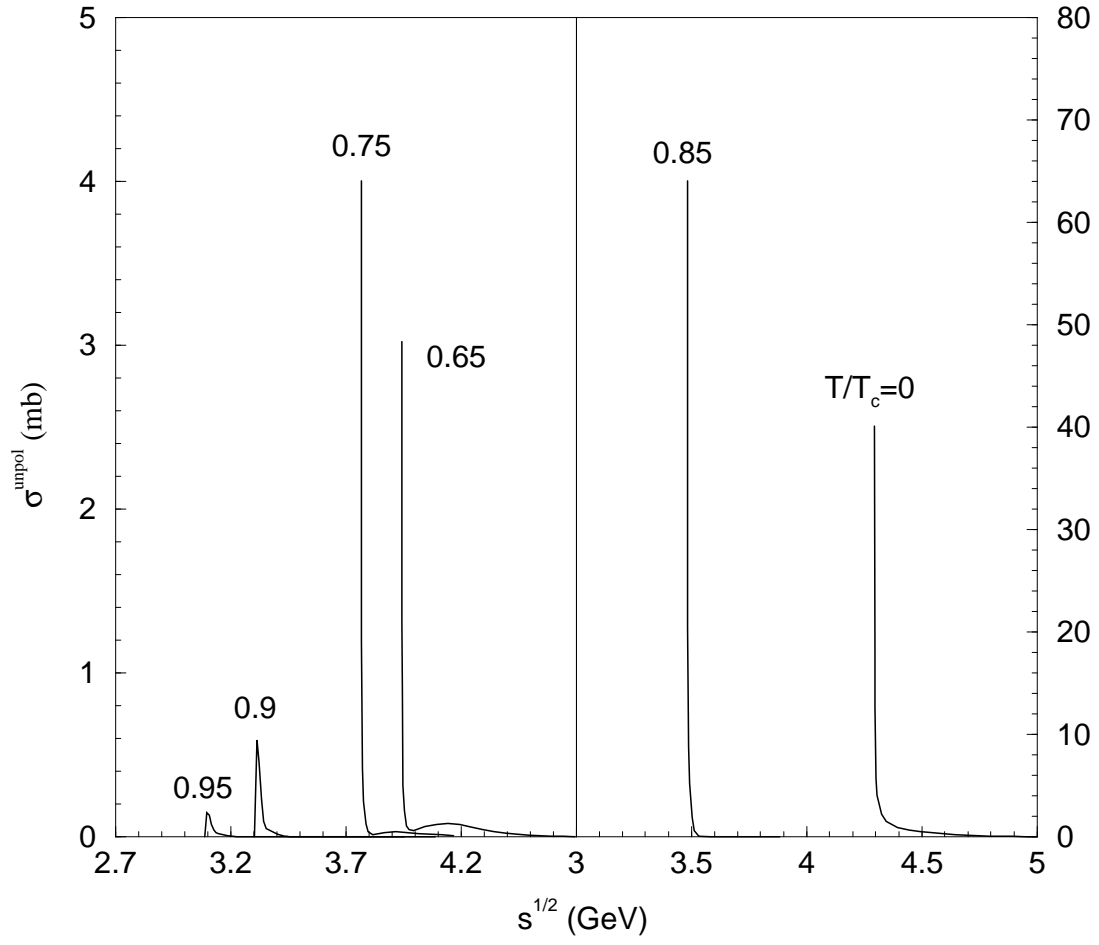


Figure 15: Cross sections for $\rho\chi_c \rightarrow \bar{D}^*D$ or $\bar{D}D^*$ at various temperatures.

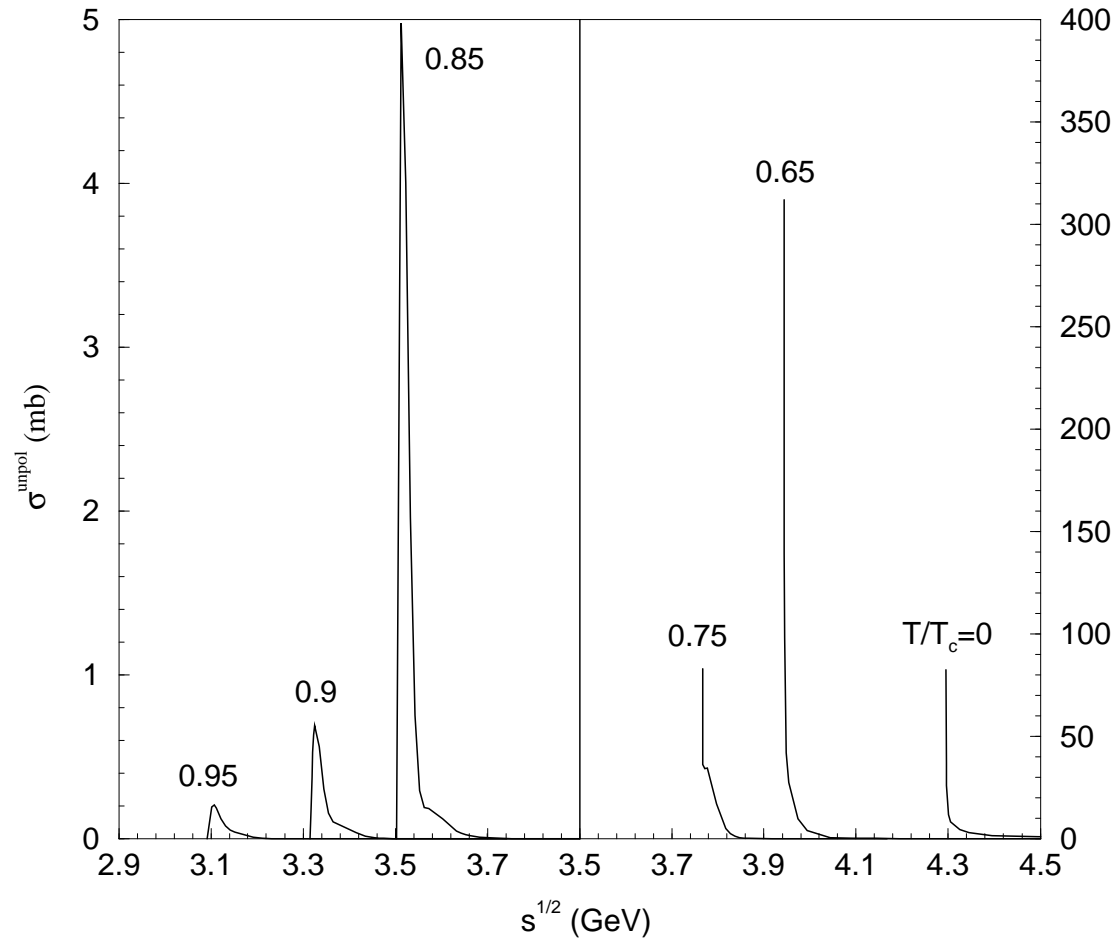


Figure 16: Cross sections for $\rho\chi_c \rightarrow \bar{D}^* D^*$ at various temperatures.

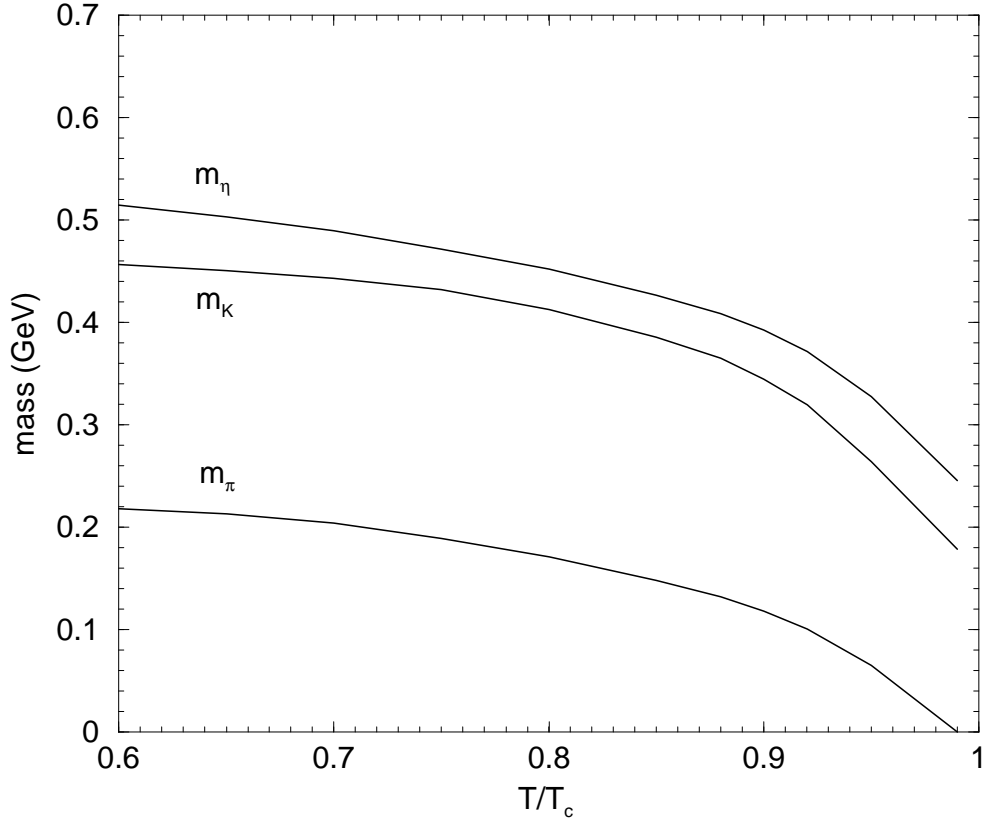


Figure 17: π , K and η masses as functions of T/T_c .

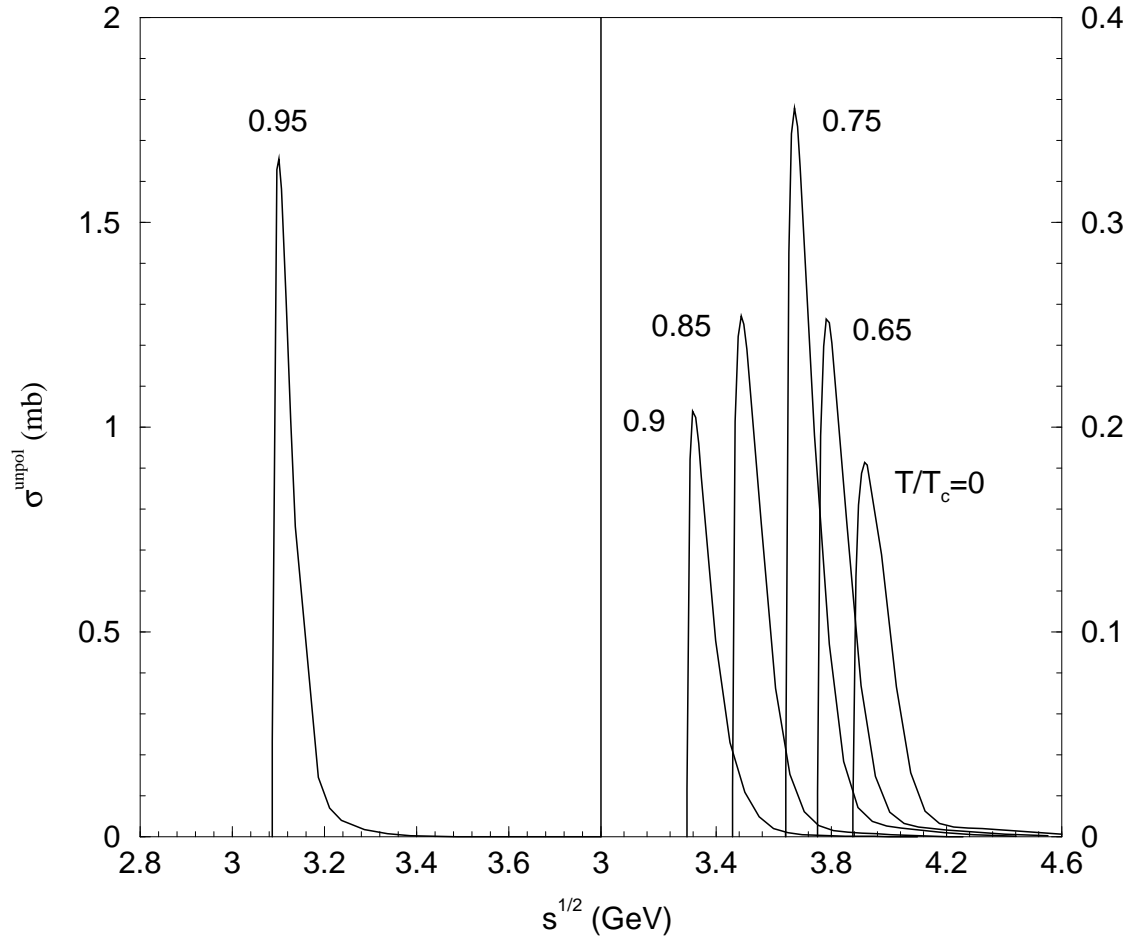


Figure 18: Cross sections for $\pi J/\psi \rightarrow \bar{D}^* D$ or $\bar{D} D^*$ at various temperatures.

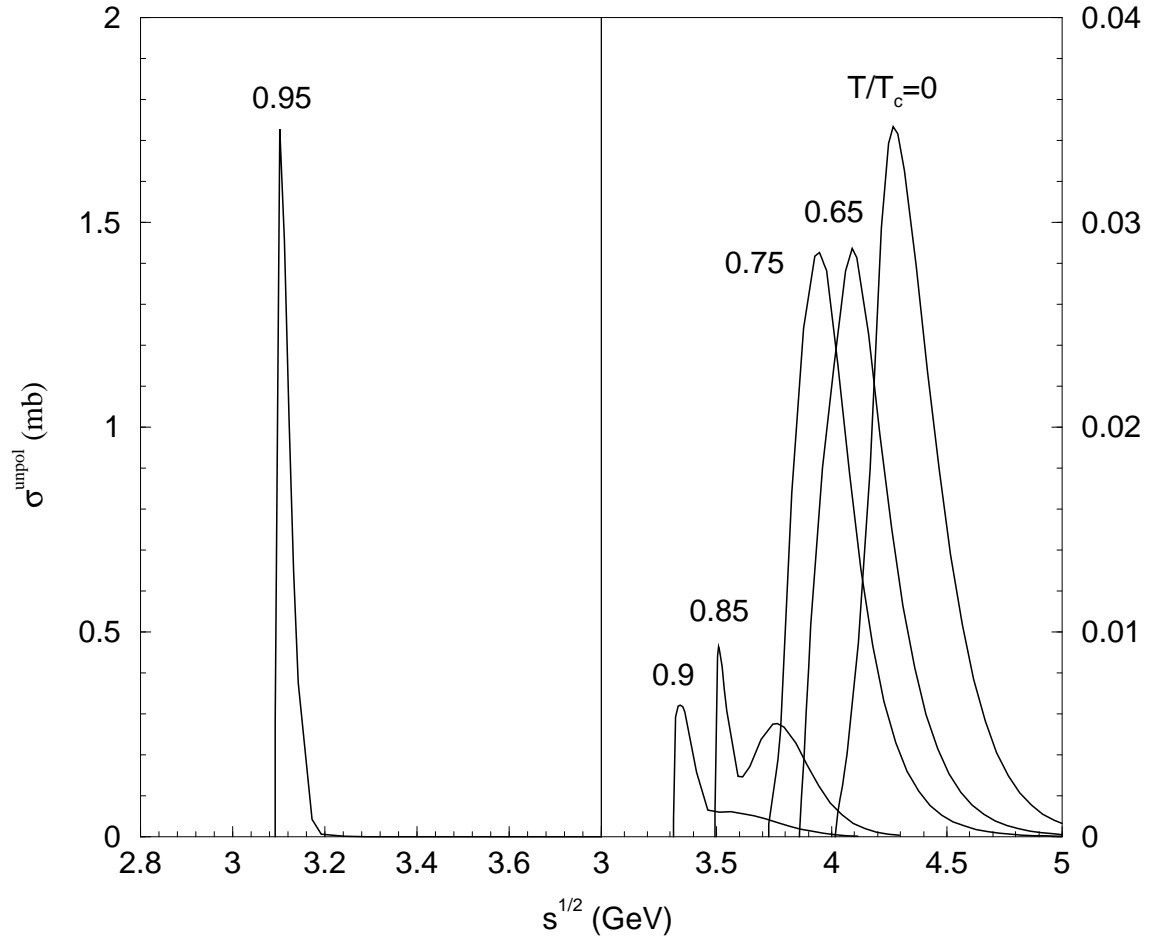


Figure 19: Cross sections for $\pi J/\psi \rightarrow \bar{D}^* D^*$ at various temperatures.

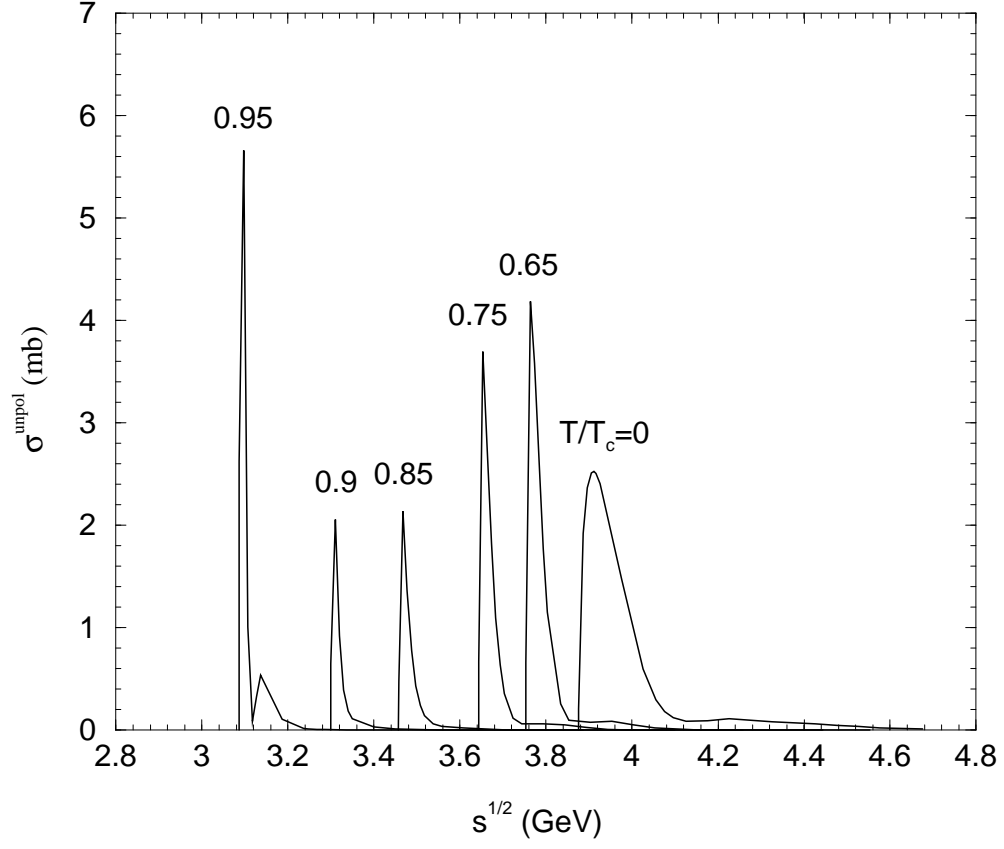


Figure 20: Cross sections for $\pi\psi' \rightarrow \bar{D}^*D$ or $\bar{D}D^*$ at various temperatures.

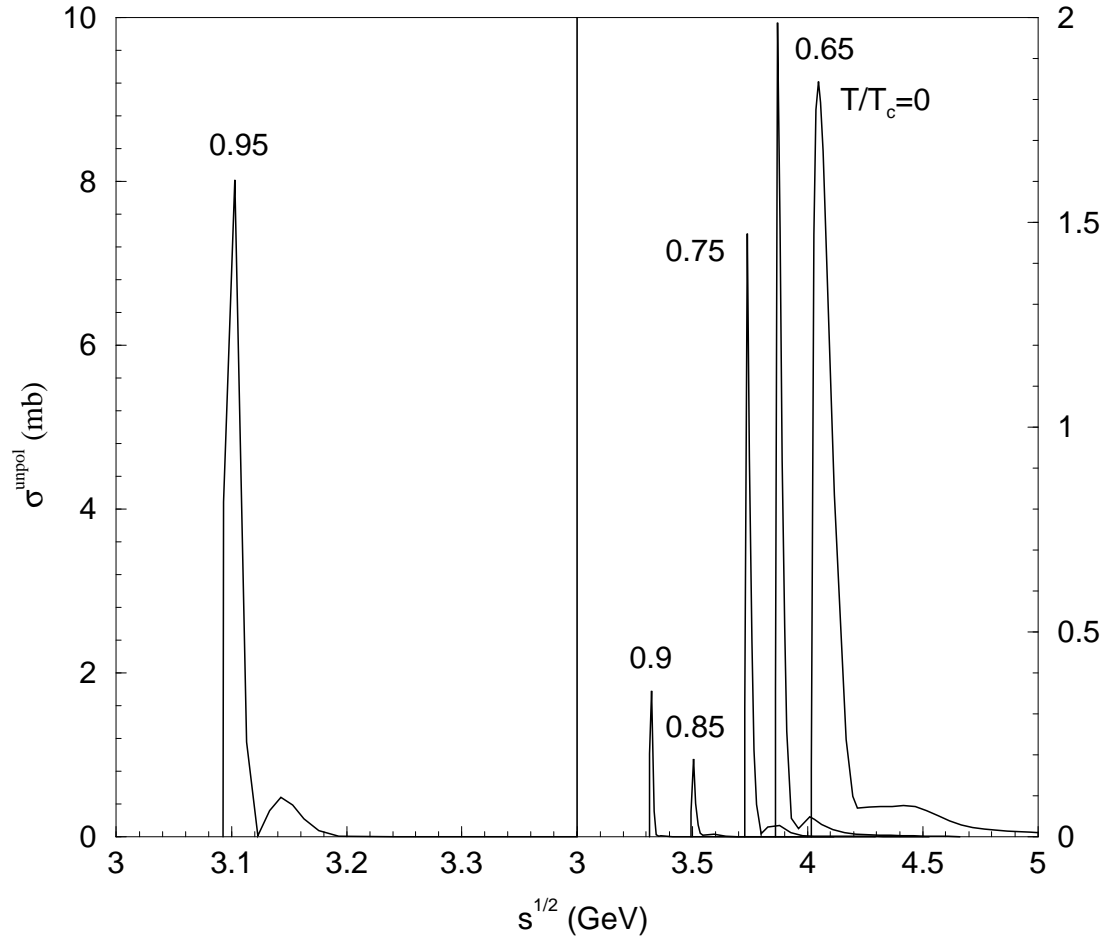


Figure 21: Cross sections for $\pi\psi' \rightarrow \bar{D}^*D^*$ at various temperatures.

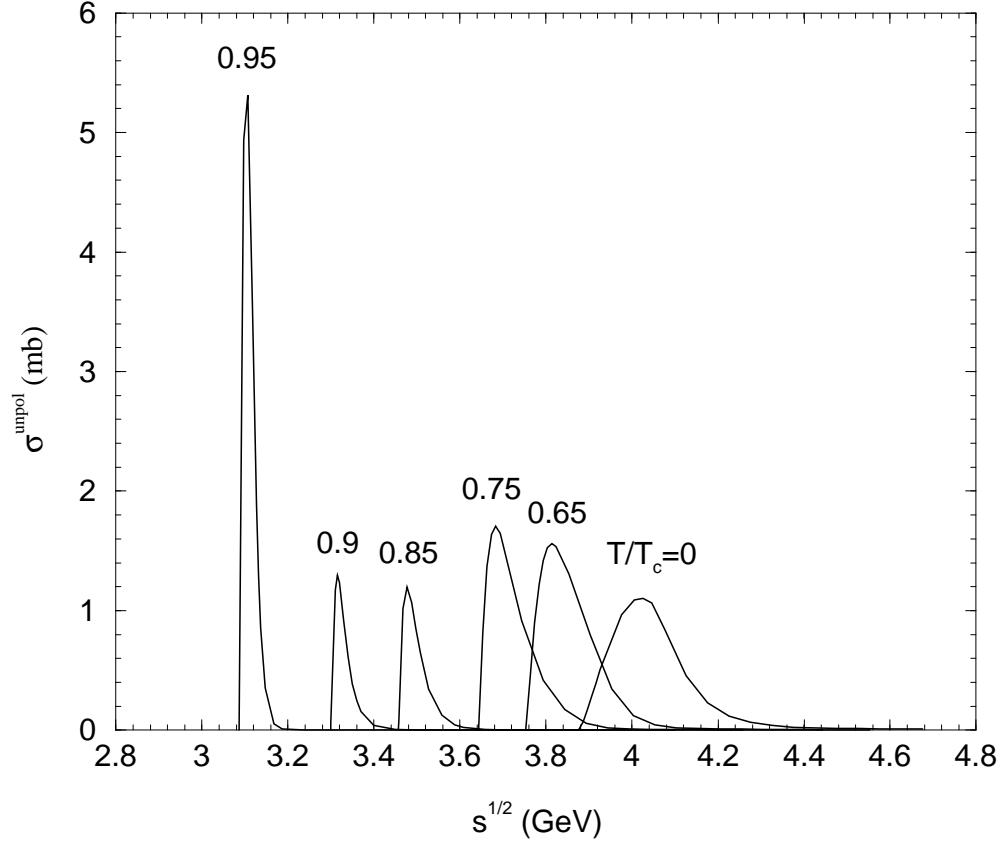


Figure 22: Cross sections for $\pi\chi_c \rightarrow \bar{D}^*D$ or $\bar{D}D^*$ at various temperatures.

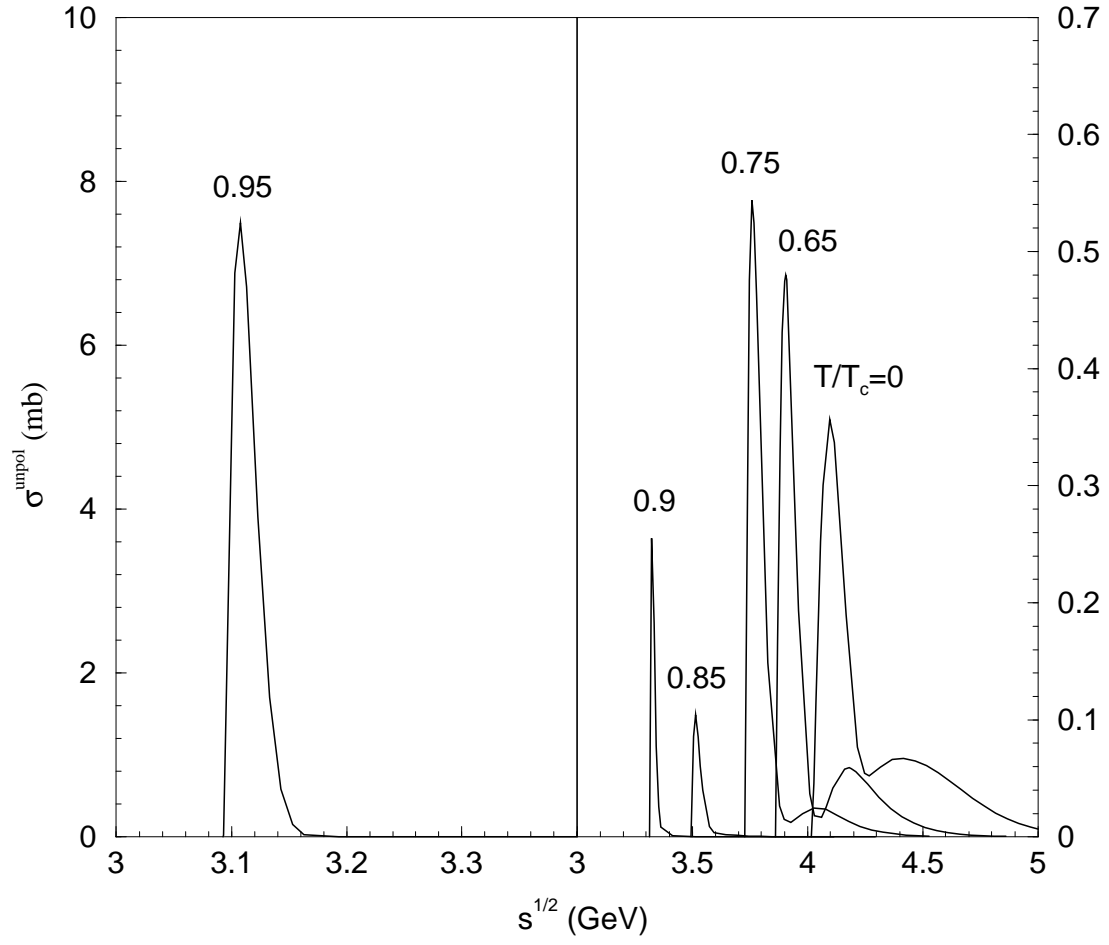


Figure 23: Cross sections for $\pi\chi_c \rightarrow \bar{D}^* D^*$ at various temperatures.

Table 1: Values of the parameters in Eq. (30) for the $\pi J/\psi$ dissociation. a_1 and a_2 are in units of mb; b_1 , b_2 , d_0 , and $\sqrt{s_z}$ are in units of GeV; c_1 and c_2 are dimensionless.

Reactions	T/T_c	a_1	b_1	c_1	a_2	b_2	c_2	d_0	$\sqrt{s_z}$
$\pi J/\psi \rightarrow \bar{D}^* D$ or $\bar{D} D^*$	0	0.16	0.03	0.53	0.05	0.08	2.42	0.04	4.556
	0.65	0.2	0.021	0.51	0.1	0.069	1.8	0.03	4.279
	0.75	0.27	0.025	0.47	0.1	0.044	0.87	0.03	4.089
	0.85	0.21	0.021	0.5	0.09	0.073	1.87	0.03	3.847
	0.9	0.18	0.015	0.51	0.08	0.069	1.75	0.02	3.649
	0.95	1.05	0.006	0.49	1	0.025	1.27	0.01	3.291
$\pi J/\psi \rightarrow \bar{D}^* D^*$	0	0.026	0.26	4.54	0.006	0.35	0.59	0.25	5.072
	0.65	0.022	0.2	2.14	0.005	0.14	0.56	0.23	4.864
	0.75	0.026	0.2	3.29	0.003	0.52	0.2	0.22	4.666
	0.85	0.01	0.016	0.5	0.006	0.27	5.09	0.02	4.287
	0.9	0.006	0.039	1	0.003	0.005	0.45	0.03	4.066
	0.95	1.61	0.007	0.54	0.45	0.026	2.78	0.01	3.187

Table 2: The same as Table 1 except for $\pi\psi'$.

Reactions	T/T_c	a_1	b_1	c_1	a_2	b_2	c_2	d_0	$\sqrt{s_z}$
$\pi\psi' \rightarrow \bar{D}^*D$ or $\bar{D}D^*$	0	1.78	0.02	0.5	1.15	0.06	1.69	0.035	4.567
	0.65	2.89	0.01	0.68	1.37	0.01	0.34	0.01	4.021
	0.75	3.18	0.01	1.11	0.61	0.01	0.01	0.01	3.871
	0.85	1.46	0.005	0.49	0.89	0.009	0.55	0.01	3.606
	0.9	1.38	0.01	5.59	0.68	0.03	0.01	0.01	3.431
	0.95	5.04	0.002	0.32	3.34	0.01	6.61	0.01	3.215
$\pi\psi' \rightarrow \bar{D}^*D^*$	0	1.6	0.025	0.5	0.3	0.042	1.66	0.03	4.78
	0.65	1.6	0.005	0.51	0.78	0.018	1.64	0.01	4.103
	0.75	1.3	0.005	0.49	0.37	0.014	1.42	0.01	3.916
	0.85	0.13	0.008	2.36	0.08	0.003	0.12	0.01	3.64
	0.9	0.35	0.005	2.23	0.36	0.002	0.28	0.01	3.349
	0.95	6.4	0.009	5.08	5	0.001	0.15	0.01	3.176

Table 3: The same as Table 1 except for $\pi\chi_c$.

Reactions	T/T_c	a_1	b_1	c_1	a_2	b_2	c_2	d_0	$\sqrt{s_z}$
$\pi\chi_c \rightarrow \bar{D}^*D$ or $\bar{D}D^*$	0	0.95	0.13	3.17	0.18	0.07	0.84	0.15	4.577
	0.65	1.13	0.07	1.78	0.5	0.04	0.71	0.06	4.135
	0.75	1.39	0.04	1.32	0.32	0.05	0.46	0.04	3.955
	0.85	1.04	0.02	1.04	0.16	0.01	0.25	0.02	3.636
	0.9	1.14	0.01	0.83	0.4	0.03	3.67	0.015	3.438
	0.95	4.51	0.017	2.03	1.32	0.01	1.05	0.02	3.167
$\pi\chi_c \rightarrow \bar{D}^*D^*$	0	0.29	0.08	2.53	0.08	0.05	1.12	0.08	5.069
	0.65	0.39	0.04	1.45	0.1	0.05	3.86	0.045	4.58
	0.75	0.45	0.03	1.6	0.11	0.05	1.17	0.03	4.293
	0.85	0.08	0.016	1.48	0.03	0.028	1.65	0.02	3.724
	0.9	0.17	0.003	2.22	0.25	0.012	1.98	0.01	3.405
	0.95	6.36	0.003	2.43	7.48	0.015	2.16	0.015	3.159

Table 4: Values of the parameters in Eqs. (30) and (32) for the $\rho J/\psi$ dissociation. a_1 and a_2 are in units of mb; b_1 , b_2 , d_0 , and $\sqrt{s_z}$ are in units of GeV; c_1 and c_2 are dimensionless.

Reactions	T/T_c	a_1	b_1	c_1	a_2	b_2	c_2	d_0	$\sqrt{s_z}$
$\rho J/\psi \rightarrow \bar{D}D$	0	0.073	0.04	0.51	0.049	0.45	5.01	0.05	4.747
	0.65	0.24	0.008	0.47	0.16	0.03	0.79	0.01	4.29
	0.75	0.22	0.01	0.41	0.11	0.01	0.54	0.007	3.676
	0.85	0.16	0.007	0.52	0.049	0.02	0.45	0.007	3.887
	0.9	0.25	0.005	0.37	0.15	0.01	1.99	0.01	3.423
	0.95	0.83	0.005	0.5	0.7	0.02	1.57	0.01	3.179
$\rho J/\psi \rightarrow \bar{D}^*D$ or $\bar{D}D^*$	0	0.71	0.03	0.39	0.56	0.42	6.42	0.03	5.011
	0.65	0.28	0.013	0.5	0.067	0.3	2.63	0.02	4.648
	0.75	0.15	0.012	0.47	0.044	0.27	3.06	0.01	4.541
	0.85	0.091	0.009	0.44	0.045	0.18	3.92	0.01	4.196
	0.9	0.28	0.005	0.38	0.15	0.006	1.49	0.01	3.6
	0.95	2.03	0.007	0.53	0.68	0.024	2.18	0.01	3.181
$\rho J/\psi \rightarrow \bar{D}^*D^*$	0	0.63	0.05	0.47	0.43	0.36	5.79	0.04	5.043
	0.65	0.086	0.06	0.46	0.043	0.28	4.05	0.04	4.901
	0.75	0.043	0.03	0.46	0.033	0.24	2.39	0.03	4.765
	0.85	0.0061	0.012	0.46	0.0031	0.14	1.6	0.01	4.291
	0.9	0.27	0.007	0.84	0.091	0.002	0.18	0.01	3.607
	0.95	5.51	0.005	0.51	4.47	0.02	1.63	0.01	3.189

Table 5: The same as Table 4 except for $\rho\psi'$.

Reactions	T/T_c	a_1	b_1	c_1	a_2	b_2	c_2	d_0	$\sqrt{s_z}$
$\rho\psi' \rightarrow \bar{D}D$	0	0.02	0.13	0.72	0.02	0.05	0.45	0.1	5.355
	0.65	0.0019	0.04	0.53	0.0012	0.25	2.74	0.03	4.848
	0.75	0.0022	0.022	0.54	0.00079	0.27	4.83	0.03	4.37
	0.85	0.049	0.01	0.52	0.047	0.021	2.76	0.01	3.575
	0.9	3.1	0.006	0.9	5.57	0.002	0.38	0.01	3.373
	0.95	1.07	0.005	0.62	0.26	0.01	0.1	0.01	3.171
$\rho\psi' \rightarrow \bar{D}^*D$ or $\bar{D}D^*$	0	0.083	0.05	0.5	0.045	0.23	1.8	0.1	5.354
	0.65	0.017	0.03	0.53	0.0043	0.3	8.68	0.03	4.818
	0.75	0.027	0.008	0.46	0.021	0.04	0.74	0.01	4.44
	0.85	3.6	0.0008	0.49	4.54	0.0046	1.27	0.005	3.568
	0.9	2.09	0.006	1.8	2.09	0.003	0.17	0.01	3.385
	0.95	0.99	0.006	0.77	0.62	0.007	0.23	0.01	3.173
$\rho\psi' \rightarrow \bar{D}^*D^*$	0	0.2	0.03	0.51	0.14	0.19	1.37	0.05	5.337
	0.65	0.78	0.05	3.08	0.04	0.0013	0.68	0.05	4.535
	0.75	10.86	0.0009	0.44	13.39	0.005	1.05	0.005	3.832
	0.85	4.79	0.005	0.82	6.23	0.002	0.48	0.01	3.597
	0.9	2.07	0.003	0.49	0.72	0.012	0.78	0.004	3.394
	0.95	2.76	0.005	0.47	1.08	0.015	0.8	0.006	3.185

Table 6: The same as Table 4 except for $\rho\chi_c$.

Reactions	T/T_c	a_1	b_1	c_1	a_2	b_2	c_2	d_0	$\sqrt{s_z}$
$\rho\chi_c \rightarrow \bar{D}D$	0	0.029	0.07	0.5	0.0073	0.21	1.24	0.1	5.173
	0.65	0.007	0.21	3.1	0.0003	0.005	0.51	0.2	4.815
	0.75	0.001	0.007	0.51	0.0008	0.24	3.59	0.01	4.306
	0.85	0.03	0.003	0.63	0.0062	0.01	0.2	0.005	3.666
	0.9	2.98	0.007	1.42	1.94	0.017	2.98	0.01	3.397
	0.95	0.52	0.009	1.54	0.32	0.019	3.15	0.01	3.203
$\rho\chi_c \rightarrow \bar{D}^*D$ or $\bar{D}D^*$	0	0.1	0.16	1.16	0.045	0.02	0.49	0.15	5.172
	0.65	0.0029	0.008	0.44	0.018	0.23	2.7	0.25	4.806
	0.75	0.0034	0.007	0.5	0.0044	0.2	3.09	0.15	4.302
	0.85	1.75	0.003	0.5	1.41	0.011	1.63	0.005	3.606
	0.9	1.58	0.01	1.4	0.81	0.015	2.03	0.01	3.433
	0.95	0.34	0.014	1.33	0.11	0.013	4.84	0.01	3.222
$\rho\chi_c \rightarrow \bar{D}^*D^*$	0	0.31	0.27	3.43	0.29	0.04	0.54	0.25	5.172
	0.65	1.91	0.005	0.52	1.87	0.024	1.55	0.01	4.44
	0.75	8.57	0.006	0.58	8.57	0.018	1.82	0.01	3.879
	0.85	2.21	0.007	1.58	1.96	0.018	3.48	0.01	3.632
	0.9	0.29	0.012	1.66	0.13	0.013	1.02	0.01	3.459
	0.95	0.11	0.013	1.99	0.041	0.025	0.76	0.01	3.231